UNIVERSITY OF SOUTHAMPTON

FACULTY OF NATURAL AND ENVIRONMENTAL SCIENCES

School of Chemistry

Fabrication of Microporous Templates For Use In Supercritical Fluid Electrodeposition (SCFED)

by

Jack Cook

Thesis for the degree of Master of Philosophy

May 2015

Abstract

This thesis described the development of microporous and mesoporous templates for use as nanowire deposition templates in Supercritical Fluid Electrodeposition (SCFED) as part of an EPSRC funded project.

This project was focussed in 3 areas of interest:

1. Growth of aluminophosphate VPI-5 crystals for mounting onto a microelectrode

Phase pure VPI-5 crystals were grown up to lengths of ~500 µm and characterised by X-ray diffraction. Freeze drying proved to be a successful method for removing water from the pores of VPI-5 without degradation of the structure, however the quantity of water removed was not ascertained. The growing of larger crystals by seeding with VPI-5 crystals was attempted with varying levels of success.

2. Growth of a thin film of zeolite SL-1 onto a TiN/Si electrode

SL-1 films were grown onto TiN/Si substrates with a wide variety of morphologies and differing levels of uniformity. These differences were caused by varying the pre-treatment of the substrates alongside the quantity of water in the autoclaves and crystallisation temperature/time. One sample in particular showed uniform coverage, providing a good basis for any future work.

3. Modification of existing anodic alumina membranes to aid SCFED

A phenyl phospohonate compound was grafted onto anodic alumina membranes of differing porosity. These membranes showed a large increase in hydrophobicity through observing the contact angle of a water droplet on the surface of the membrane. A regular membrane readily absorbs water, whereas a grafted membrane shows significant hydrophobicity.

1 – Project Objectives and Literature Review

1.1 – Objectives

1.1.1 – Microporous Zeolitic Crystals as SCFED Templates

By restricting access to an electrode surface through use of a porous, non-conducting template, electrodeposition can be used in the growth of wires. Conventionally, surface tension of electrolytes prevents access to the smallest of pores in the range of a few nanometres in diameter.

Deposition into nanometre diameter porous templates results in the growth of nanowires. Owing to their size, nanowires could potentially be used in shrinking component sizes (ie. transistors) as well as possessing different properties to their bulk counterparts such as resistance and crystallinity. As such, to access these smaller pores a different type of electrolyte is needed.

Supercritical fluids are substances which are above their “critical point”, whereby they are above a temperature at which they can behave as a liquid but simultaneously at pressures at which they cannot behave as a gas. The resulting fluid flows as a gas but can dissolve like a liquid, albeit with reduced solubility by comparison to conventional solvents. A complete lack of viscosity allows for permeation into even the smallest of pores. With the use of co-solvents, supercritical fluids have been used as electrodeposition electrolytes to access small pore templates.

This project looked to provide suitable hosts to test the small pore limits of the technique. This required a pore size of 1-2 nm, uniform pore size distribution, no electrical conductivity, chemical and thermal stability under supercritical conditions, parallel alignment of pores, and (ideally) a lack of interconnecting pores (i.e. a network). For extremely small pore sizes such as these target materials were recognised to be likely to possess an inherent nanoporosity through crystallinity.

Zeolites have consistent, ordered porosity due to their crystalline nature and use of structural directing agents (SDAs) and, as such, were suitable candidates to meet the above criteria. Pore sizes over 1 nm can come with several drawbacks in that some larger pore

zeolitic systems are only stable with template molecules adsorbed and are thus unsuited for SCFED, whereas others are extremely complicated to synthesise and single crystal growth is particularly challenging. Careful literature research was needed to identify a suitable system.

A common technique to grow larger single crystals is by seeding with fragments of existing crystals. Syntheses of single crystals of complicated systems often produce high quantities of impurity phases, so a technique was also required to separate crystals from impurities for seeding in further reactions to grow larger crystals.

1.1.2 – Growth of Zeolitic Thin Films

Initial work was to be directed towards growth of a randomly oriented microporous zeolitic film on TiN before focussing on the synthesis of oriented films. Ideally, with an oriented film the pores of the template would be uniformly aligned in a perpendicular arrangement with respect to the place of the TiN substrate.

As described previously the larger pore zeolites tend to be composed of Al/Si and Al/P mixtures, however for the purpose of film growth using a single source precursor (SiO_x) presents less problems than a dual source counterpart (AlO_x/SiO_x).

1.1.3 – Modification of Anodic Alumina (AAO) Membrane

The final area of the project was to alter the properties of AAO. Although membranes of various pore diameters had been successfully used as templates for SCFED the extent of water content was problematic and in some cases (Ge deposition) limiting.

Inverting the hydrophilicity of alumina would not only address this issue but also present the opportunity to alter the properties of deposited material in the pores due to interactions with the pore walls.

As AAO membranes tended to possess pores of >13 nm in diameter the shrinkage in size by grafting groups would be minimal so any alterations in properties would stem from interaction between deposited material and grafted groups.

For this section of the project a reliable, non-aqueous grafting process was desired. Likely candidates would be phosphorus based compounds due to their ease of formation and strength of potential Al-O-P linkages which could be formed on alumina substrates.

1.2 – Electrodeposition

Electrodeposition is the growth of a material on an electrode surface from an electrolyte upon passage of a current. Using a chemically/thermally stable, porous, non-conducting template restricts access to the electrode surface exclusively through the pores. However, upon decreasing the aforementioned pore size to a number of nanometres presents a limitation; surface tension of the electrolyte prevents pore access. Supercritical fluids possess both the properties of a liquid and a gas, behaving as a solvent yet with almost zero viscosity. Furthermore, some fluids possess a large potential window for electrodeposition and their properties can be fine-tuned by alteration of operating temperature and pressure. With this ability to access the smallest of pores due to a lack of viscosity, it is therefore logical to test the limiting pore size of a template at which deposition can still occur. [1–6]

1.3 – Microporous Zeolitic Systems

Zeolitic systems are defined as ordered porous materials with an inorganic, 3-dimensional host structure composed of fully linked, corner-sharing tetrahedra (IUPAC). As aforementioned, the challenging aspect of growing zeolitic systems of diameter >1 nm stems from the unusually large rings that are needed to encompass the pores, which can subsequently cause issues with stability. A pore is referred to as being “extra-large” if it is surrounded by 12 or more oxygen atoms. [7–11]

The ITQ germanosilicate subset of zeolites presents numerous examples of extra-large pores. ITQ-33 possesses 3D channels of 18 x 10 x 10 atoms formed by double 4 rings (D4Rs) and 3 ring (3R) secondary building units (SBUs), crystallises in a hexagonal space group and has good thermal stability. For SCFED, a material with 3D channels (as opposed to 2D - such as ITQ-33) could be used as it still would test the limits of pore size access. Figure 1 depicts the pore structure of ITQ-33, highlighting (in blue) the composite building unit shared with another extra-large pore zeolite ITQ-44. [9,10,12–14]

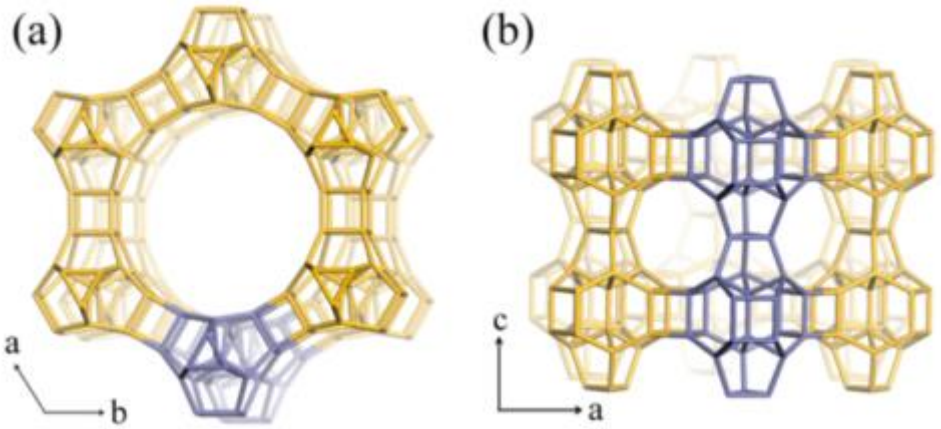

Figure 1 – ITQ-33 pores viewed along the (a) c and (b) b axes, with the former showing the ~1.3 nm pore aperture. Reprinted with permission, Copyright 2013 American Chemical Society [11]

Alteration of the Si/Ge ratio in the synthesis gel in turn changes the resulting morphology. At higher Si/Ge ratios of 5:1 and 4:1 clusters of nanofibres form, whereas at a 1:1 ratio hexagonal platelets form suggesting that the former high Si gels cause stacking defects upon crystallisation due to the rigidity of the Si-O units in comparison to Ge counterparts.

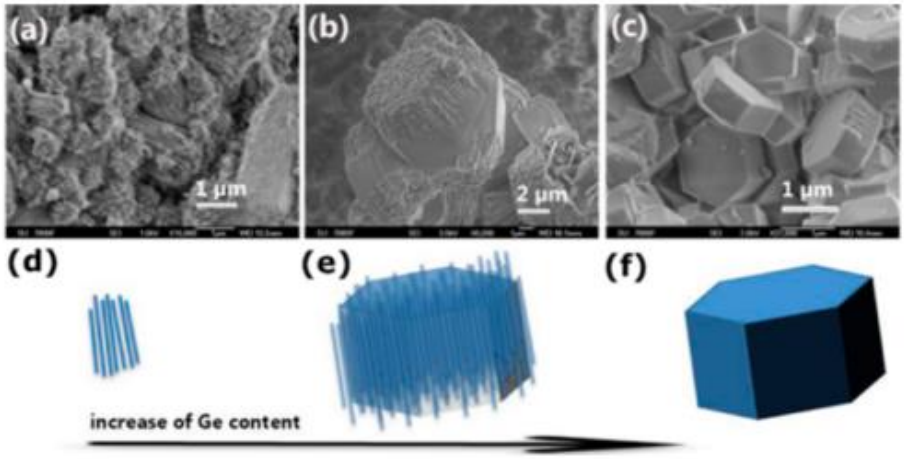

Figure 2 – SEM images of ITQ-33 grown using Si:Ge ratios of (a) 5:1, (b) 4:1 and (c) 1:1. Reprinted with permission, Copyright 2013 American Chemical Society [11]

At higher Si contents ITQ-33 forms a hierarchical structure with micropores within each fibre and mesopores between each fibre, these mesoporous gaps between fibres are ideal for increased diffusion and better access to micropores. However, for the purpose of a supercritical fluid electrodeposition template, the deposition would preferably occur in the

mesopores due to easier diffusion to the electrode surface compared to micropores. As such, a 1:1 ratio of Si:Ge would be more useful for a deposition template to eliminate any mesopores. [12]

Following on from the syntheses of microporous ITQ-33 and mesoporous ITQ-37, which are comprised of D4R and D3R SBUs respectively, it was postulated that a structure containing both D4Rs and D3Rs would have an even lower framework density; this lead to ITQ-40, a zeolite with extra-large 16 x 15 x 15 T-atom pores. [8,12,15]

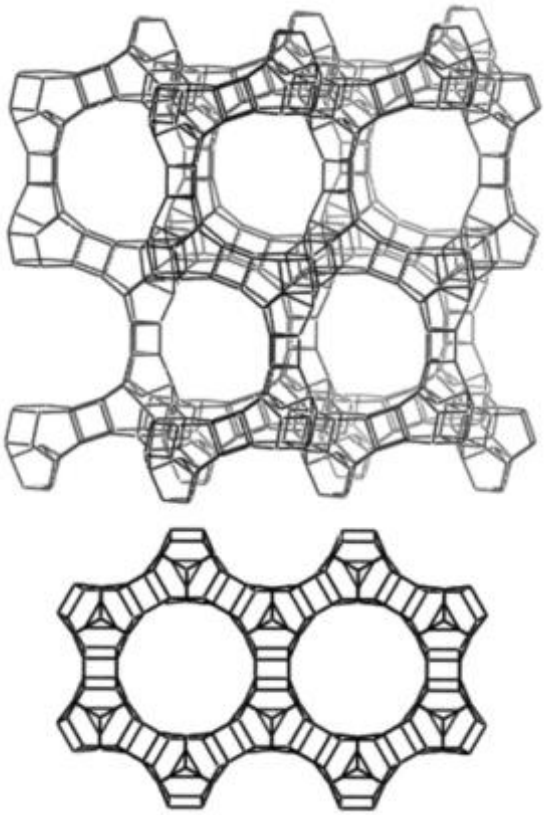

Figure 3 – ITQ-40 pore structure along the [100] direction of the 16 ring pores (above) and along the [001] direction of the 15 ring pores (below). Reprinted with permission from PNAS, Copyright 2010 [8]

Again in a similar fashion to ITQ-33 a Si:Ge ratio of 1:1 is required, in addition to 1 molar equivalent of water, to synthesise phase pure ITQ-40. Figure 3 shows the pore structure as synthesised, with a ~1 nm circular 15 ring along [001] and ~0.94 x 1.04 nm elliptical 16 rings along the [100] and [010] respectively.

Upon removal of the Et_2Ph_2POH structure directing agent (SDA) the pores of ITQ-40 collapse, preventing its use as a deposition template.[8]

Another ITQ structure utilising both D3R and D4R building units is ITQ-44, a silicogermanate which shares several characteristics with ITQ-33. Instead of 18 x 10 x 10 ring pores of ITQ-33 it possesses 18 x 12 x 12 ring pores. Instead of 3 ring (3R) building units, where T atoms are either Al or Si, germanium is substituted allowing formation of D3R building units. The 18 ring channel in both ITQ-33 and ITQ-44 is approximately 1.25 nm whereas the diameter of the interconnecting channels from the 10 and 12 rings are ~0.4x0.6 nm and ~0.8x0.6 nm respectively. [7,12]

Alongside germanium, several other bi- and trivalent species can replace silicon and aluminium in zeolites to enable the formation of extra-large pore structures. ECR-34, an aluminium gallium silicate zeolitic system, possesses one dimensional pores of ~1 nm formed by 18 membered rings and is stable to 800 ^{o}C. To prevent the formation of phase impurities such as faujasite and zeolite L concentrations of the sodium, potassium and tetraethyl ammonium (TEA) cations are vital. Figure 4 depicts the pore structure of ECR-34 along the c axis. [16]

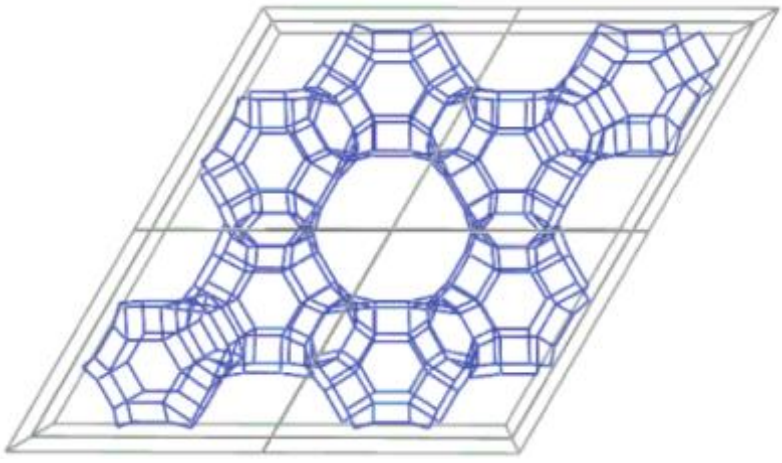

Figure 4 – ECR-34 viewed down the c axis showing 18-ring channel. Reprinted with permission, Copyright 2003 American Chemical Society [16]

The slightly puckered arrangement of the ring, in addition to deviation from a planar structure, results in the smaller pore diameter of ~1 nm as opposed to an expected 1.5 nm diameter from a perfectly planar 18 ring channel. [16]

Significant drawbacks to the ITQ and ECR structures include the complexity of the gel and the required reaction conditions. ECR-34 in particular requires 7 components to the gel, including 3 cations, and a 17 day synthesis. UTD-1, a high silica zeolite of pore diameter ~1x0.75 nm, requires a highly complex SDA. Ideally a target zeolite would have a shorter crystallisation time, a less complex gel and a simple SDA to enable easier experimentation with single crystal growth. [8,12,13,15,17,18]

Aluminophosphate VPI-5 shares several pore characteristics with ECR-34 in the fact that both possess one-dimensional pores formed by 18 atom rings. By contrast, in the case of VPI-5 the ring is more planar in structure and as such possesses a larger pore size of 1.21 nm, with the pores being arranged in a parallel fashion with no interconnecting micropores of >0.4 nm in diameter between these channels. Moreover, the gel is composed of an alumina source, a phosphate source, SDA and water with a crystallisation time of 24 hours. It is an unusual aluminophosphate as the organic structure directing agent is not present in the pores post-synthesis, due to the hydrophilic nature of the pores. Figure 5 shows the similarities between $AlPO_4$-5 and VPI-5 of the AFI and VFI zeolitic structures respectively. [19–26]

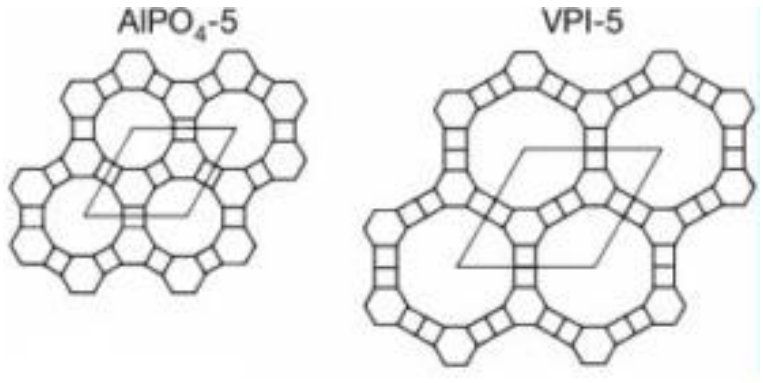

Figure 5 – Pore structures of $AlPO_4$-5 and VPI-5, adopting the AFI and VFI structures respectively. Reprinted by permission from Macmillan Publishers Ltd: Nature, Copyright 2002 [27]

However, the nature of the 2 double 4 rings (D4R) bridging hexagonal rings in VPI-5 is that they are arranged in a cis geometry. Thus, small tetrahedral Al units joining the D4Rs are strained with 90^o angles between Al-O bonds, which is a highly unstable arrangement. To

accommodate this arrangement, Al atoms co-ordinate with 2 chemisorbed water molecules, forming a pseudo-octahedral unit of $Al(O)_4(H_2O)_2$. Figure 6 highlights this arrangement; note that 2 overlapping rings are shown, with 3 Al atoms in each layer (alternating pairs of D4Rs) co-ordinating an extra 2 water molecules for stability. [13,26–30]

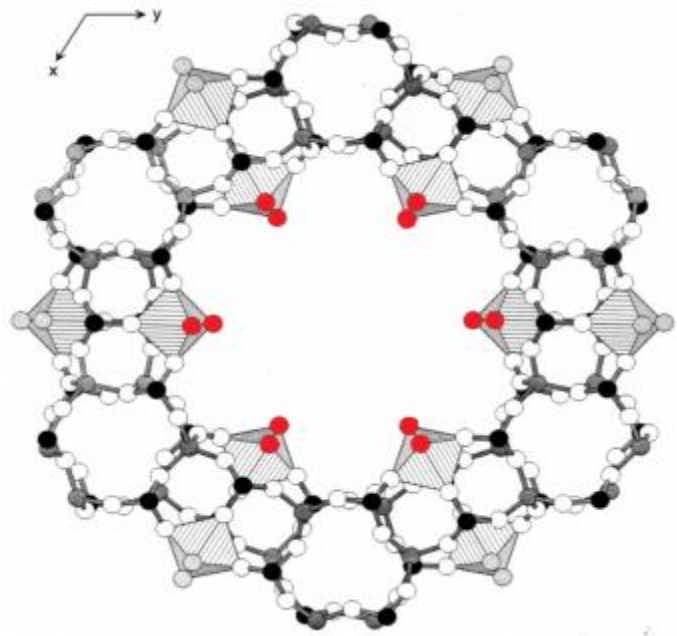

Figure 6: Two layers of the 18 T-atom pore structure of VPI-5, 3 Al atoms in each layer have two additional chemisorbed water molecules in their co-ordination spheres (red). Reprinted with permission from Elsevier, Copyright 2000 [31]

Some difficulties have been described in the literature with VPI-5 synthesis, with common phase impurities being: AlPO-41, AlPO-H1/2/3, and AlPO-8, thus thorough characterisation of this material is crucial for complete phase identification. There are a few factors which are ubiquitous across the syntheses such as templating agent and crystallisation temperature, so a certain degree of standardisation does exist for the preparation of VPI-5.[19,22–28,30–39]

The aforementioned hydration of VPI-5 has also been proven to be problematic in the literature, due to the instability of the structure upon dehydration. As the pores of VPI-5 are occupied with chemisorbed water as well as a central triple helix of physisorbed water; removing the water under atmospheric pressure results in the structure collapsing to the smaller pore AlPO-8 as shown in figure 7. However, there are reports of the ability to dehydrate VPI-5 under vacuum or supercritical conditions whilst retaining the pore

structure, with a reduction in unit cell symmetry from $P6_3$ to C_m (shown in figure 8). Furthermore, these dehydrated samples are reported to be of a high thermal stability. There are also reported cases whereby washing samples of VPI-5 with alcohols (methanol, ethanol) further improved upon the thermal stability of VPI-5. [21,28,31,38,40]

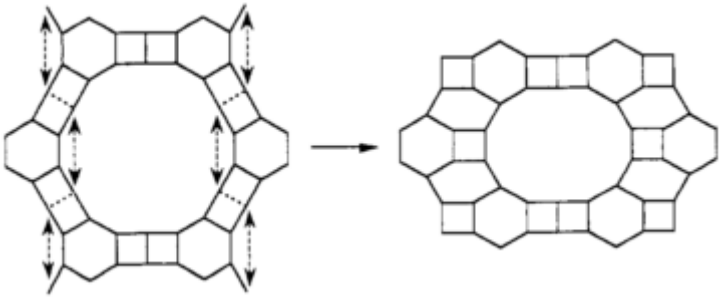

Figure 7 – degradation of VPI-5 to AlPO-8 upon removal of chemisorbed and physisorbed water. Reprinted with permission, Copyright 2013 American Chemical Society [23]

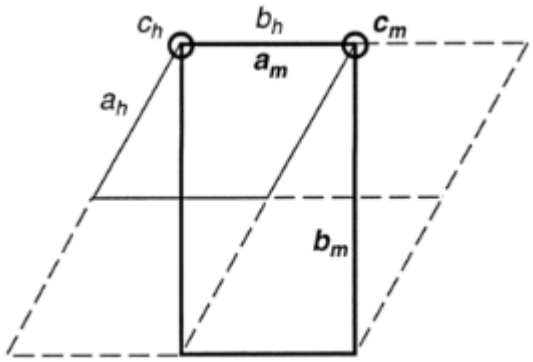

Figure 8 – Reduction in unit cell symmetry of VPI-5 from $P6_3$ hexagonal to C_m monoclinic, Reprinted with permission from Elsevier, Copyright 2000 [31]

VPI-5 possesses adequate pore dimensions and properties to be used as a deposition template and as such is a desirable target system to grow as a single crystal. Research by McCusker et. al details the single crystal growth of VPI-5 through stringent hydrothermal conditions required to promote large crystal growth, in particular high dilution, homogenous mixing of the gel, low crystallisation temperature and the use of polyphosphoric acid as a P source. Use of a polymeric source of phosphorus may facilitate single crystal growth by slower release of nutrients into the gel. [8, 21-22]

Figure 9 depicts the "wheat sheaf" type crystals grown at 135 ^{o}C (below standard conditions for VPI-5 synthesis) which appear to be densely intergrown needles from a central

nucleation point. Reported yields appeared to be very good and a consistent crystal size and shape was obtained.

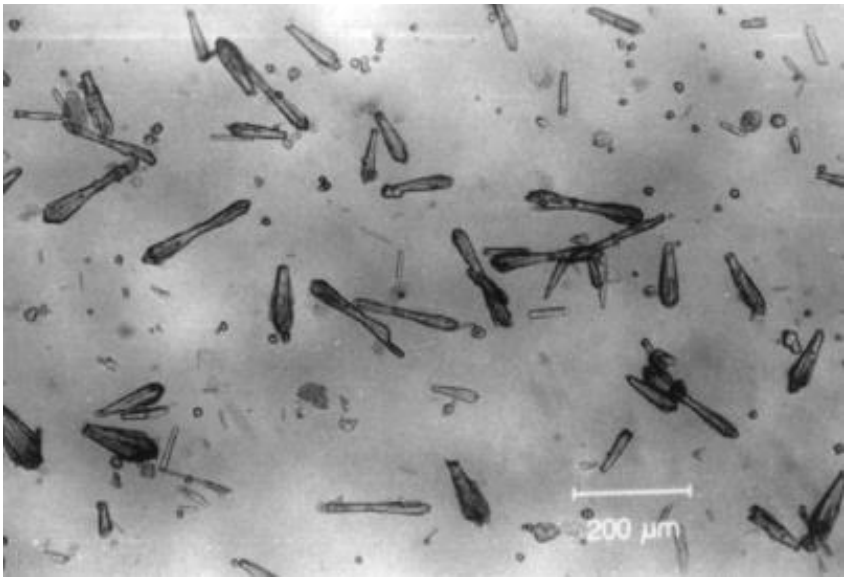

Figure 9 – Wheat sheaf clusters of VPI-5 crystals. Reprinted with permission from Elsevier, Copyright 1999 [37]

Figures 10 and 11 depict an individual needle grown at a much lower temperature of 125 ^{o}C, evidently far below standard conditions for VPI-5 synthesis.

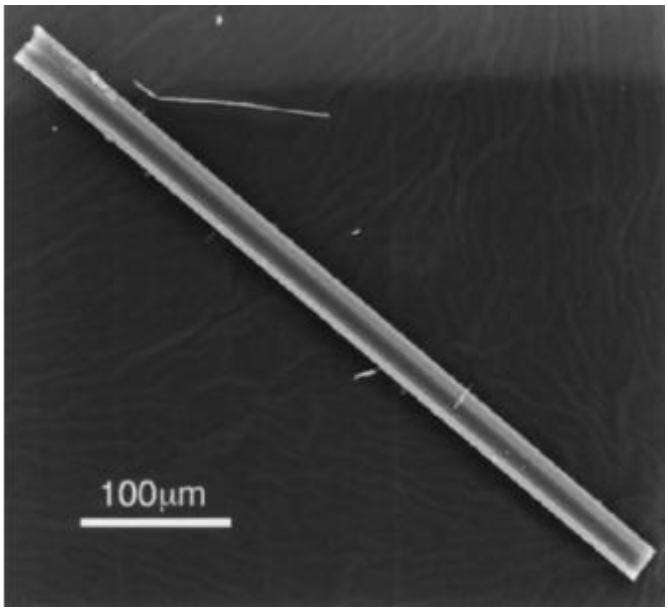

Figure 10 – Single needle of VPI-5. Reprinted with permission from Elsevier, Copyright 1999 [37]

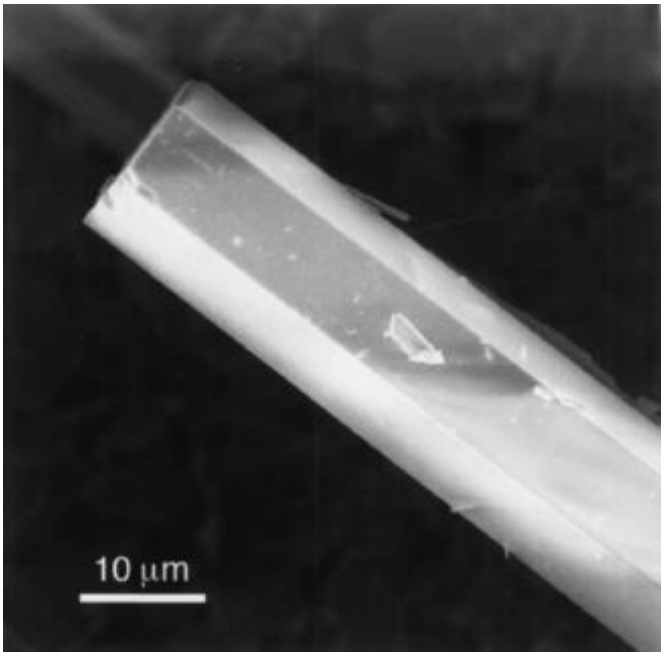

Figure 11 – Closer view of VPI-5 needle, showing hexagonal crystal growth. Reprinted with permission from Elsevier, Copyright 1999 [37]

These appear to be singular, longer crystals of VPI-5 evidently hexagonal in shape, reflecting the VFI $P6_3$ hexagonal unit cell. The size and shape of these crystals corresponds well with proposed ideal single crystal growth conditions, use of a lower temperature. Due to the low amount of energy available it becomes more favourable to grow an existing crystal as opposed to nucleating and forming a new cluster.

1.4 – Growth of Thin Films of the Zeolite SL-1

Previous work in literature described the growth of polycrystalline, randomly oriented films of silica only zeolite silicalite-1 (hereon referred to as SL-1). SL-1 possesses pores of ~ 0.55 and 0.56 nm in the a and b directions respectively; the pores in the b direction are straight and parallel to one another, whilst the pores in the a direction are interweaved between the b directional pores and exhibit a zig-zag shape. SL-1 also crystallises in a variety of morphologies. [41–45]

The process is based on coating a substrate with a SiO_x precursor, and in the case of SL-1 using tetrapropylammonium hydroxide (TPAOH) as a template. Upon hydrothermal treatment, the amorphous silica precursor is directly transformed into a zeolitic film bound to the substrate. 2 methods were used by the research team at University College London (UCL): Steam assisted crystallisation (SAC) and vapour phase transportation (VPT).

SAC, depicted in figure 12, involves directly applying template solution to the surface of the substrate before crystallisation and having the substrate facing upwards during the process. Upon reaching hydrothermal conditions the vaporised water initiates film growth.

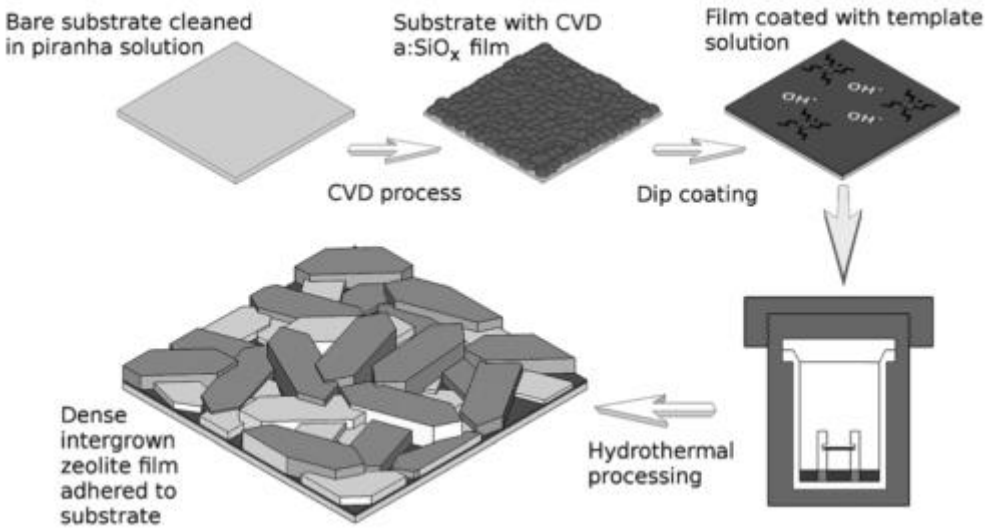

Figure 12 – SAC process for growth of a polycrystalline zeolitic film. Reproduced with permission of The Royal Society of Chemistry [44]

In contrast, VPT requires the substrate face downwards, again suspended from the Teflon insert as in SAC, with the template dissolved in the amount of water at the bottom of the

Teflon liner. Upon reaching hydrothermal conditions the template is transported to the surface of the substrate via vapour phase.

It is also known that SL-1 can crystallise in a variety of morphologies, as shown in figure 13 below. [45]

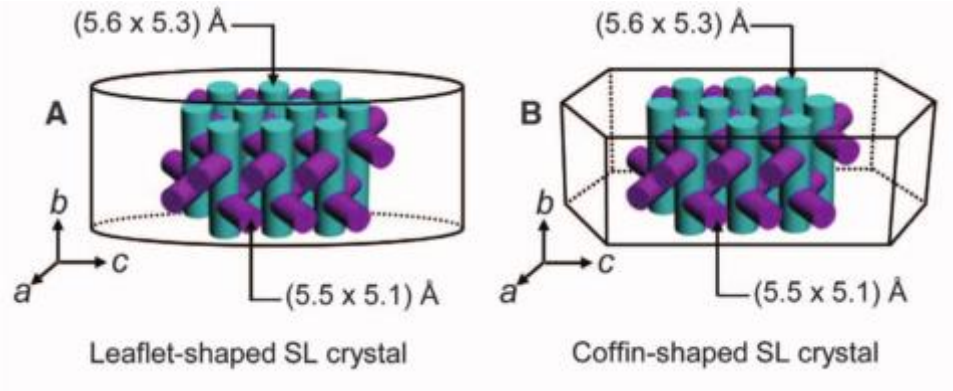

Figure 13 – Morphologies and pore dimensions of SL-1. Reprinted with permission from AAAS [45]

The process was successful on both aluminium and silicon substrates, denoting a lack of substrate sensitivity for the process and thus potential for a TiN substrate which is one of the electrode materials used for SCFED. [44]

A drawback of a polycrystalline substrate is shown in figure 14 below, as gaps between crystallites will be easily permeated by a supercritical fluid instead of the smaller pores.

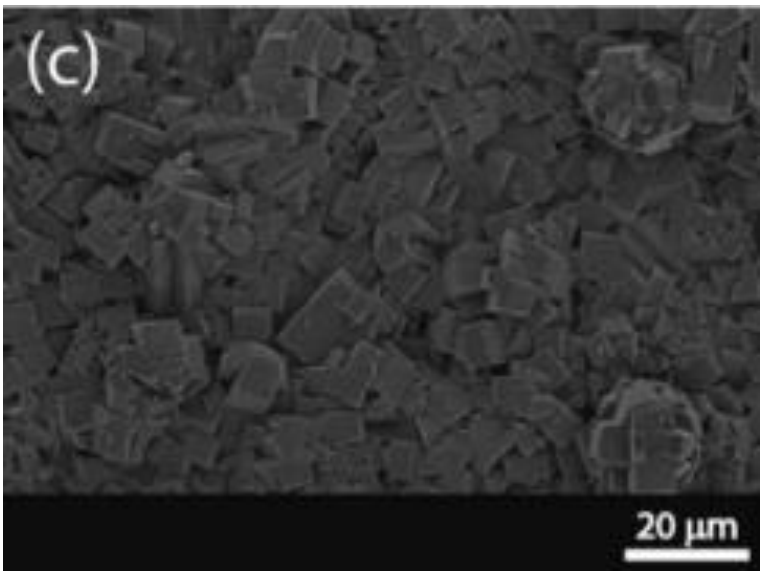

Figure 14 – SL-1 film grown on alumina. Reproduced with permission of The Royal Society of Chemistry [44]

Evidently, if the desired deposition were to occur in the pores, the gaps between crystals would have to be eliminated in their entirety by growth of a uniformly oriented film. Fortunately, there have been numerous reported cases of success in growing oriented films of SL-1 by the use of seed crystals, illustrated in figure 15. [42,43,45–48]

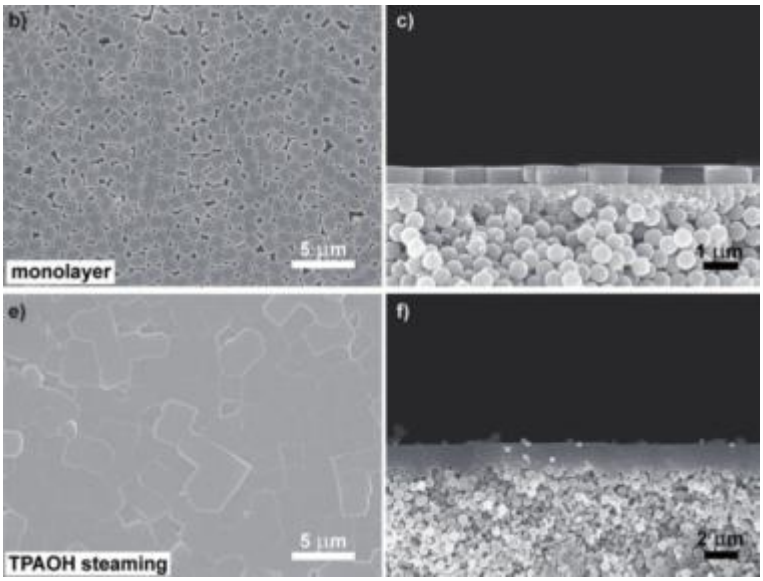

Figure 15 – SEM images showing from above (b, e) and side on (c, f) SL-1 crystals mounted on a Si substrate before (b, c) and after (e, f) steam assisted film growth. Copyright 2013 Wiley-VCH [42]

A substrate is coated with SiO_x beads as described previously and a single layer of SL-1 seed crystals are mounted on top. This monolayer mounting can be performed by a variety of techniques, the simplest being by application of SL-1 crystals using a fingertip of a glove. [45,49–52]

Upon hydrothermal treatment in the presence of template solution, the amorphous SiO_x fills the gaps inbetween the monolayer of seed crystals and then by secondary growth the film grows towards the substrate. This was shown by both SEM and XRD to produce highly ordered SL-1 films. [42,46,53]

A noticeable drawback for use as a substrate can be identified by looking at the SEM images from figure 15, as the film thickness tends towards 100-200 nm. Given that the pore size of

SL-1 is in the region of ~0.5 nm this gives rise to an extremely high aspect ratio. Even with the capabilities of supercritical fluids it could prove problematic to deposit along pores of that aspect ratio. Moreover, if any amorphous SiO_x remained unreacted it would likely be that closest to the substrate, as such this would act as an insulating layer between template and electrode.

1.5 – Grafting Hydrophobic Groups into Anodic Alumina (AAO) Membranes

It is well known that, under acidic pH and electrochemical control, porous anodized alumina can be formed with well-defined, continuous, parallel pores. As it is an insulating material with a controllable pore diameter it has been used extensively in the SCFED project as a template. [1–6,54]

However, several precursor materials such as those of germanium are known to be highly moisture sensitive. Alumina possesses surface bound hydroxyl groups and consequently is highly hydrophilic in its nature. This evidently can cause several problems for moisture sensitive reagents.

Efforts have been made to dry templates under vacuum, but in some cases it has not been sufficient. By changing the hydrophilic nature of anodic alumina to hydrophobic it could not only solve the problem of hydration of SCFED precursors, it could also lead to different properties of deposited materials due to the varying functional groups lining the pores.

There are ample examples of functionalising alumina surfaces, all of which have a variety of reaction conditions. Of particular interests were those performed in non-aqueous conditions. By utilising the favourable formation of the Al-O-P bond from Al-OH precursors, phosphates and their derivatives are useful target grafting groups. Phosphonates ($R\text{-}P(O)(OR)_2$) share similar structural properties to phosphates through a mutual phosphoryl P=O and 3 further substituents. However, in contrast to 3 P-O-R linkages, phosphonates possess just 2 P-O-R linkages alongside a P-C bond. This is a particularly stable bond and allows for attachment of organic groups without the issue of possible cleavage that P-O-R groups suffer from. [55–58]

2 – Experimental

2.1 – VPI-5 Synthesis

2.1.1 – Gel Preparation and Hydrothermal Synthesis

Reagents were measured out to the molar ratio of: 1 Al_2O_3 : 1 P_2O_5 : 1 DPA/DBA : xH_2O; whereby DPA/DBA is the templating molecule di-n-propylamine/di-n-butylamine, and x denotes the molar quantity of water factoring in that contributed by the alumina and the phosphoric acid. Note that the fill level of the autoclaves was ~75 % or ~96ml in 125ml liner.

For the purpose of simplicity, the procedure described below is of the successful phase pure VPI-5 sample JC/025b. Table 1, overleaf, describes the underlined variables encountered in each step. Refer to section 5.2.1 for the full sample database detailing variables experimented with for each sample produced.

Step 1

- Pural SB boehmite (6.697 g powder = 5.123 g, 50.24 mmol as Al_2O_3) was slurried in H_2O [a](27.5 ml, 1528 mmol) by [b]pestle and mortar.
- Separately, [c]polyphosphoric acid (8.255 g → 7.132 g, 50.24 mmol as P_2O_5) was heated to reduce viscosity and added to the slurry whilst [b]grinding, using H_2O [a](3 x 1 ml, 167 mmol) to aid the addition of any residue.
- The resulting hydrogel was [d]sonicated for 30 minutes producing a viscous gel.

Step 2

- Whilst [e]stirring, the second quantity of water [f](53.1 ml, 2949 mmol) was added alongside [g]di-n-propylamine (5.084 g, 50.24 mmol) and the gel was left to age for [h]30 minutes.

Step 3

- A 125 ml Teflon liner was charged with the gel and placed in a stainless steel Parr autoclave, and crystallised at [i]135^{o}C for [j]24 hours.

Step 4

- The product was washed with 3 x H_2O and 1 x ethanol before drying at room temperature.

Variable	Step	Description
a	1	Quantity of water added
b	1	Manual grinding or magnetic stirring
c	1	Use of ortho or poly phosphoric acid
d	1	Optional sonication step
e	2	Stir speed in RPM
f	2	Quantity of water added
g	2	Organic templating agent
h	2	Ageing time
i	3	Crystallisation temperature
j	3	Crystallisation time

Table 1 – Variables in VPI-5 synthesis

One significant difference from the literature was the use of manual grinding by pestle and mortar instead of an agate ball mill. This presented challenges in reproducibility and consistency between samples.

2.1.1 – Density Separation

Due to foreseeable effort in growth of larger crystals by use of seeded growth, separation of zeolitic crystals from their impurities was an area of interest.

VPI-5 as-synthesised contains ~25 % water by mass, whereas impurities of dense $AlPO_4$ by-products would contain significantly less water. As the density of $AlPO_4$ is ~2.6 gml^{-1}, a VPI-5 framework with 25 % mass as water would be less dense.

Figure 16 shows a density separation setup, which uses a solvent of intermediate density between the 2 phases to be separated, allows for one phase to simply float whilst the other sinks due to lower and higher densities than the solvent in question. [59]

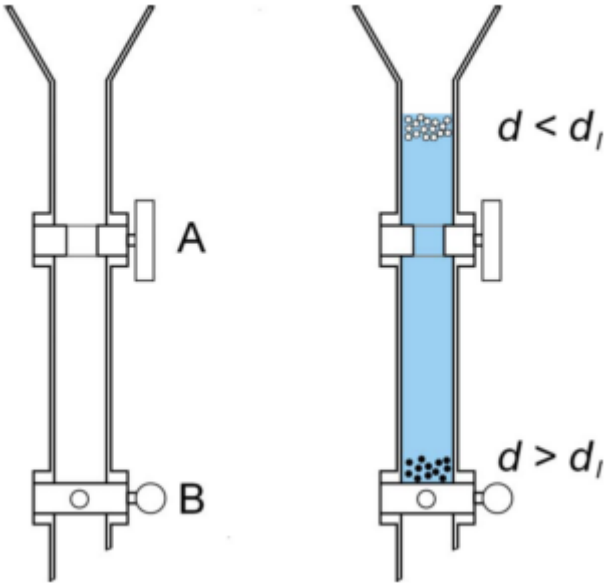

Figure 16 – Diagram depicting density separation by careful selection of solvent. Reproduced with permission of The Royal Society of Chemistry [59]

As bromoform has a density of ~2.9 gml^{-1} and is miscible with chloroform, which has a density of ~1.5 gml^{-1}, it would appear to be possible to achieve a mixture where VPI-5 would float and more dense impurities would not.

2.2 – SL-1 Thin Film Growth via SAC (Steam Assisted Crystallisation)

Piranha solution was produced by adding 1.25 ml of >30 % wt/vol H_2O_2 to 3.75 ml of 98 % H_2SO_4 and stirred by pipette to initiate the reaction. Once the solution had settled, substrates were immersed for a set period of time and then placed in water for 5 minutes prior to washing with ethanol.

For SAC a (cleaned) TiN/Si wafer coated with 200 nm SiO_2 beads was coated in tetrabutylammonium hydroxide (TBAOH) template by dropping pipette and spread evenly. Referring to the setup described in section 3.2 the wafer was placed with the template coated SiO_2 facing upwards on the Teflon insert. The appropriate quantity of water was added to the bottom of the liner and then the autoclave placed in an oven for a particular time at variable temperatures. To remove TPAOH, the substrates were calcined post-synthesis.

2.3 – Anodic Alumina (AAO) Membrane Grafting

2.3.1 – Grafting Agent Synthesis

It was decided that diethylphenylphosphonate would be the target grafting group. The synthesis of the precursor was straightforward as was the grafting; moreover, grafting was performed in dried DCM, facilitated by the solubility of the diethyl groups. [56]

It should be noted that diethylphenylphosphonate is described as having ~50 % coverage of the total surface of alumina in the literature, however their calculations were based on assumed area covered per bound phosphonate group and are subject to speculation. In either case, it is a feasible moisture-free grafting process for coating AAO membranes. [56]

Many other potential phosphonate grafting groups exist, and the phenyl functional group itself is open to further modification. Given a reliable grafting procedure, there are numerous possibilities for SCFED alteration through manipulation of AAO template properties.

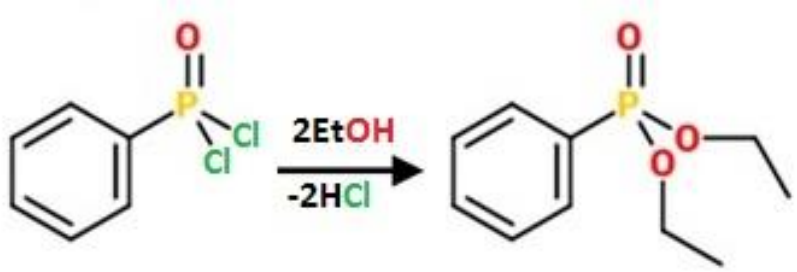

Figure 17 – Synthesis of grafting reagent from phenylphosphonic dichloride

A Schlenk tube was charged with phenylphosphonic dichloride (Sigma, 90 %, 20 ml, 0.127 mol) and cooled over ice whilst stirring rapidly. Ethanol (Absolute, 13 ml, 0.223 mol) was added in aliquots of 5/4/4 ml allowing the reaction to cool between each addition. Schlenk tube was placed under vacuum to aid removal of HCl gas and drive to completion.

Note that upon further use of grafting agent, the Schlenk tube was placed under vacuum, upon which HCl gas was liberated due to residual dissolved HCl.

2.3.2 – Grafting Process

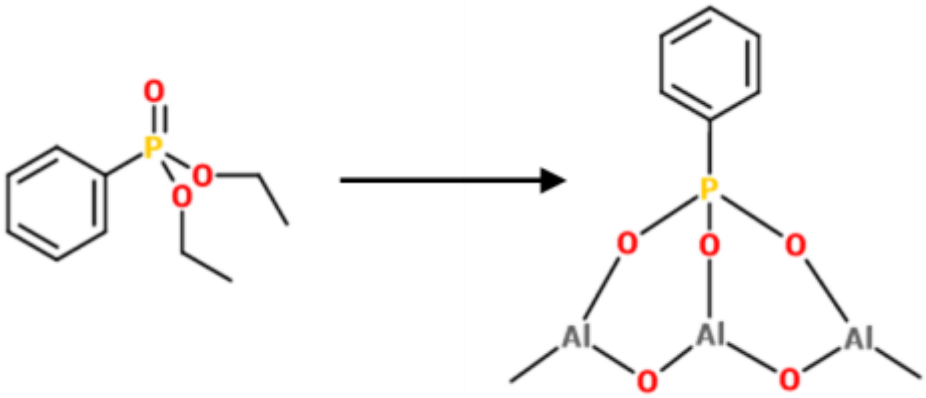

Figure 18 – Postulated method of phosphonate grafting onto alumina, note that the tetravalent phosphorus is suggested to possess an additional delocalised bond shared between the 3 P-O linkages [56]

The AAO template (13, 55 or 200 nm pore diameter) was placed in air sensitive reflux apparatus, using a 3 necked round bottom flask (RBF) with a Young's tap and a condenser also fitted with a Young's tap. After evacuating through the RBF tap and refilling with nitrogen 3 times, the template was dried under vacuum at 140 ^{o}C for 5 hours. The RBF Young's tap was closed and nitrogen filled through the condenser Young's tap.

Grafting agent from section 2.3.1 (0.75 ml) was added through a rubber septum in a side neck of the RBF followed by distilled dichloromethane (40 ml). The reaction was brought to reflux in an oil bath at 75 ^{o}C under nitrogen flow for 48 hours.

Note that whilst dichloromethane boils at 40 ^{o}C, vigorous refluxing at a higher temperature enabled better solution mixing.

The reaction mixture was removed via needle and syringe maintaining moisture free conditions, and the template was washed over with methanol (5 x 5 ml) disposing of the solvent in each wash. The membrane was finally dried under vacuum at 120 ^{o}C for 4 hours.

3 – Results and Discussion

3.1 – Aluminophosphate VPI-5

3.1.1 – Syntheses

Please refer to the sample database in the appendix for the individual sample numbers described herein. Note that samples JC/001-003 were testing single crystal growth of $AlPO_4$-5 and as such are not described herein or in the database. Furthermore, steps 1/2 in the following section refer to the steps described in section 2.1.

To begin with, the synthesis in the paper (McCusker et. al [37]) was followed but using orthophosphoric acid in an attempt to make a VPI-5 powder, as in theory this would be easier to characterise and avoid the initial difficulty of handling polyphosphoric acid.

Samples JC/004-007 were unfortunately over diluted (double) with regards to the ratio of water to Al/P reagents and as such did not form any crystalline product.

As the paper described mixing using an agate ball mill with polyphosphoric acid, it was decided that using orthophosphoric acid and magnetic stirring would be used in both ageing steps to attempt to exert control over reaction conditions in the absence of a ball mill. Orthophosphoric acid is considerably easier to measure and handle, and magnetic stirring speed can be controlled by varying RPM.

However, despite several variations of stirring speed in both ageing steps, the use of manual grinding in step 1 by pestle and mortar, ageing time, stirrer bar size, sonication and the structure directing agent, the best yield using orthophosphoric acid was ~50% VPI-5. At this point it became apparent that orthophosphoric acid, at high dilutions, was not suitable for synthesising VPI-5 single crystals. It should be noted that orthophosphoric acid can be used to make VPI-5 powder however in much lower dilutions. There is evidence to suggest that in higher dilution gels, if the phosphorus nutrients are released too rapidly into the gel, other zeolitic systems form preferentially.

Therefore, polyphosphoric acid (PPPA) was used hereon for synthesis. Polyphosphoric acid was synthesised by adding 3 equivalents of P_2O_5 powder to 1 equivalent of 85 wt% H_3PO_4,

accounting for hydration of the latter, and stirring to form PPPA with average chain length n of 8 as per literature. [37]

For the following samples, homogeneity of the gel became the main issue. Use of a magnetic stirrer bar was not sufficient to break up polyphosphoric acid, subsequently producing an unmixed gel which did not give any results upon crystallisation. Samples JC/014 and JC/019 both demonstrated that manual grinding was superior, however with the use of orthophosphoric acid it seemed to have a negligible effect on the resulting phase.

With sample JC/025, using polyphosphoric acid in addition to grinding the gel manually made a smooth low viscosity gel which thickened upon sonication. Crystallisation at 135 ^{o}C resulted in phase pure VPI-5, the powder diffraction pattern (illustrated in figure 19) as a comparison to an ICSD pattern.

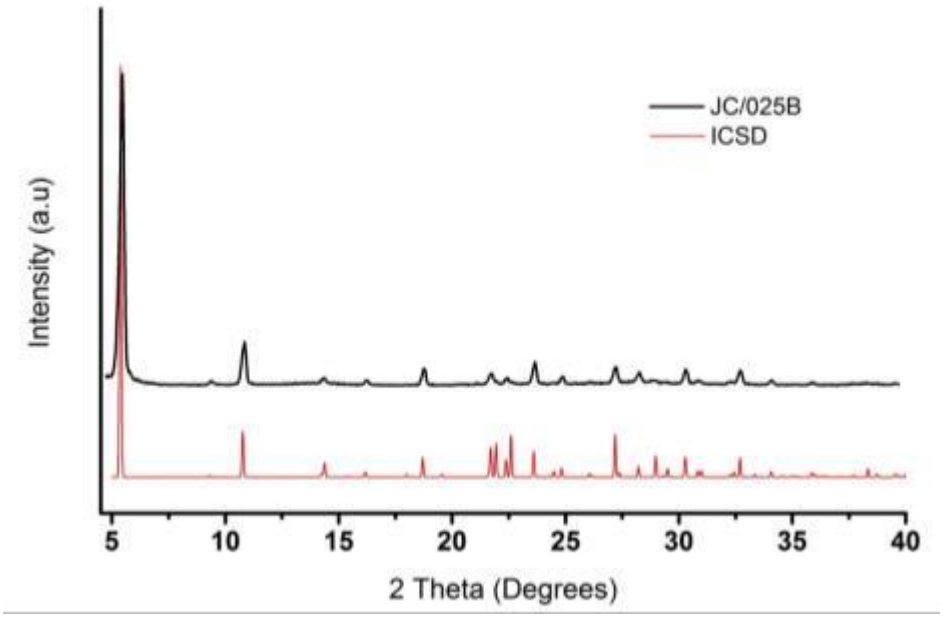

Figure 19 – Stacked XRD patterns comparing JC/025 with ICSD pattern for VPI-5

This sample was our first successful attempt at synthesising VPI-5 at high dilution. The use of polyphosphoric acid, manual grinding, sonication and a fixed ageing time are reliable for formation of a homogenous gel. Repeating identical conditions in JC/026 produced exactly the same phase pure VPI-5 sample.

An overnight scan on a laboratory diffractometer was refined, shown in figure 20. A LeBail profile fit was performed instead of a full Rietveld refinement, for two reasons. Firstly, for a

full structural refinement, a parallel beam diffraction pattern (synchrotron, neutron) provides much more accurate data with regards to atom locations in comparison to X-ray diffraction; as oxygen is abundant in all AlPOs and of relatively low electron density, so of low X-ray scattering strength, this is particularly important. Secondly, the AlO_4/PO_4 tetrahedra are flexible in themselves, requiring rigid body constraints to prevent refinement into nonsensical crystal structures.

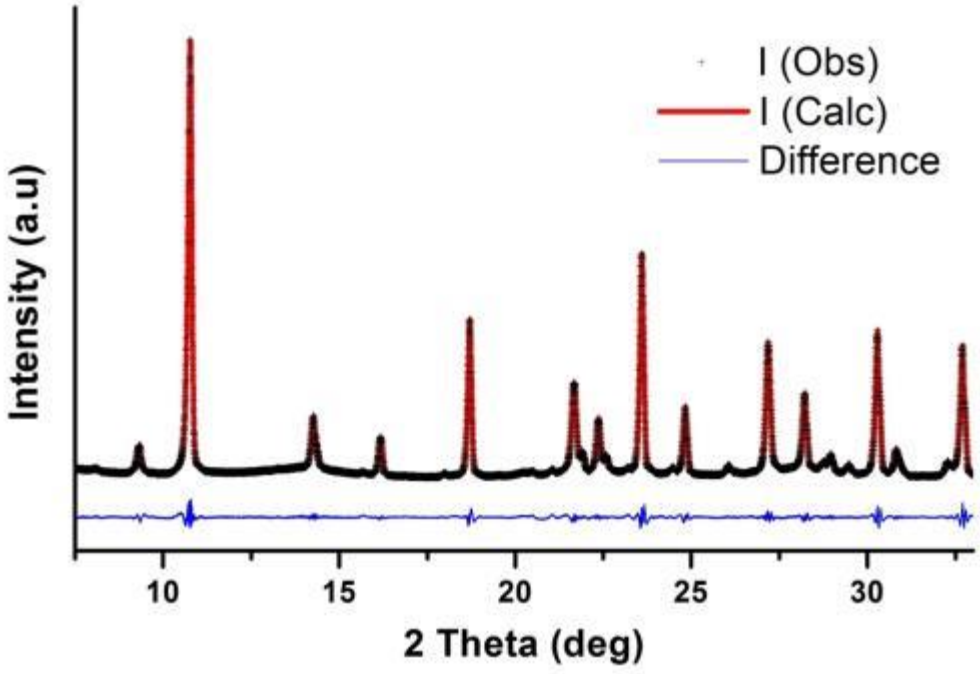

Parameter	Value (JC/025b)	Value (Literature)
a	18.9508	18.9752(1)
b	18.9508	18.9752(1)
c	8.0967	8.1044(1)
α	90	90
β	90	90
γ	120	120
Wrp	0.051	0.086

Figure 20/ Table 2 – LeBail profile fit of JC/025b against VPI-5 pattern (ICSD collection code 66164 [60]), the low angle region was removed to enable a good fit for the background function/ Corresponding refined crystal structure parameters compared to the literature [60]

Lowering the crystallisation temperature in the oven to 123 ^{o}C and 125 ^{o}C in JC/027 and JC/028 respectively produced unreacted gel and $AlPO_4$-H3 in the former and an additional,

fractional amount of VPI-5 in the latter. It must be said, however, that measuring the exact temperature inside the autoclaves was very difficult, as a 2 ^{0}C difference in temperature may not be reflected in the temperature inside the Teflon liner.

Interestingly, by changing just the crystallisation temperature, similar differences in morphology were observed between JC/025 and JC/028 at 135 ^{o}C and 125 ^{o}C, respectively, as shown in figures 21 and 22.

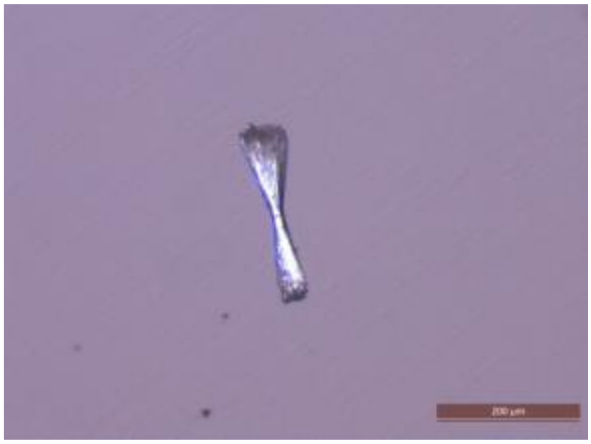

Figure 21 – JC/025b, VPI-5 synthesised at 135 ^{o}C, scale is 200 µm

Figure 22 – JC/028, Individual needle of VPI-5 synthesised at 125 ^{o}C, scale is 200 µm

Much like the “wheat sheaf” and individual needle morphologies described previously, through control of crystallisation temperature alone, the VPI-5 crystals formed change noticeably. Again at a lower crystallisation temperature nucleation is slower, leading to the preference for more individual needles as opposed to densely intergrown clusters. Note that by visual inspection only a small fraction of JC/028 was needle shaped crystals with the

rest of the sample being small spherical impurities. Analysis by X-ray diffraction showed a broad range of zeolitic products, including $AlPO_4$-H2, with little useful information, analysis of the needle crystals is detailed in section 3.1.5 (single crystal diffraction).

3.1.2 – Dehydration

In an ideal situation, the pores of an electrodeposition template would be absent of water. Not only is this important with regards to moisture sensitive deposition precursors, it also avoids any issues of the pores being blocked in the first instance.

As VPI-5 is approximately ~25 % water by mass as synthesised, dehydration is challenging. Moreover, as aforementioned in section 1.3, the pores of VPI-5 are occupied by a triple helix of water in the centre as well as chemisorbed water forming pseudo-octahedral Al on the framework itself. Removal of the latter under atmospheric conditions collapses the structure to $AlPO_4$-8 causing stacking defects. [19,23,25,27,33,36,38]

Referring to the sample database in section 5.2.1.2, several types of dehydration conditions were employed in an effort to see how VPI-5 crystals behaved relative to literature reported for powdered VPI-5 under dehydration. These samples were all fractions of phase pure VPI-5 JC/025 or JC/026 to begin with. A control experiment was performed at atmospheric pressure at 130 ^{o}C to demonstrate full conversion to $AlPO_4$-8.

To potentially reduce the pressure exerted on the pores through the collapsing of a meniscus of liquid water, the use of a vacuum was attempted to remove water with even less force exerted on the framework as it would potentially be removed in gaseous form. A vacuum, produced via an oil pump, was applied for 90 minutes before increasing the temperature to 50 ^{o}C for 50 minutes. After a final 120 minutes at 65 ^{o}C the sample was purged with N_2. Upon reapplying vacuum no bumping of the powder was observed denoting no more water could be removed under those conditions. This still showed partial conversion to $AlPO_4$-8.

To assess the effectiveness of molecular sieves, a sample was dried using sieves (dried beforehand at high temperature) for 24 hours before placing under vacuum for 1 hour followed by an increase to 100 ^{o}C for 1 hour. This again showed similar degradation as before.

In a further attempt to reduce degradation, a sample was dried under vacuum for 4 hours before treatment at 100 ^{o}C for 1 hour. This showed markedly less conversion to $AlPO_4$-8 however a significant amount of VPI-5 was still degraded. An attempt to dehydrate a sample under vacuum alone for 8 hours at room temperature showed much less degradation and retained a majority of VPI-5 phase, as shown later in figure 23 (JC/033).

It should, however, be noted that retention of VPI-5 phase does not guarantee a good level of dehydration. It is known that different types of physisorbed water exist in the pores of VPI-5. Moreover, as the chemisorbed water is a vital part of the framework, it would be the most difficult to remove. In literature it is stated that, upon removal of chemisorbed water from VPI-5, the structure reduces in symmetry from $P6_3$ to C_m (see figure 8) as the framework contorts in absence of stable $Al(O)_4(H_2O)_2$ pseudo-octahedra. [21,28,31,38,40]

It appeared that even under vacuum too much stress was being applied to the pores upon removal of water causing them to collapse. As a solution freeze-drying was attempted, where a sample is taken below 0 ^{o}C and then placed under vacuum to sublime water from solid to gas, negating the formation of a liquid meniscus and thus reducing stress on the structure.

Several combinations of freeze drying were attempted, with varying levels of success. Freeze drying samples between –18 ^{o}C and –1 ^{o}C all retained the VPI-5 phase fully. So to push this technique further, it was attempted to freeze dry a sample at – 4 ^{o}C for 4 hours as before, but to take the sample to 100 ^{o}C post drying under vacuum. Unfortunately this resulted in heavy degradation to $AlPO_4$-8 despite prior freeze drying.

Sample JC/037 proved to be of the most interest, as after freeze drying at -4 ^{o}C for 4 hours the sample was allowed to warm to room temperature and left under vacuum under the same conditions as JC/033. As shown in figure 23, the freeze drying prevents any noticeable degradation by comparison despite both samples JC/033 and JC/037 being exposed to an identical vacuum.

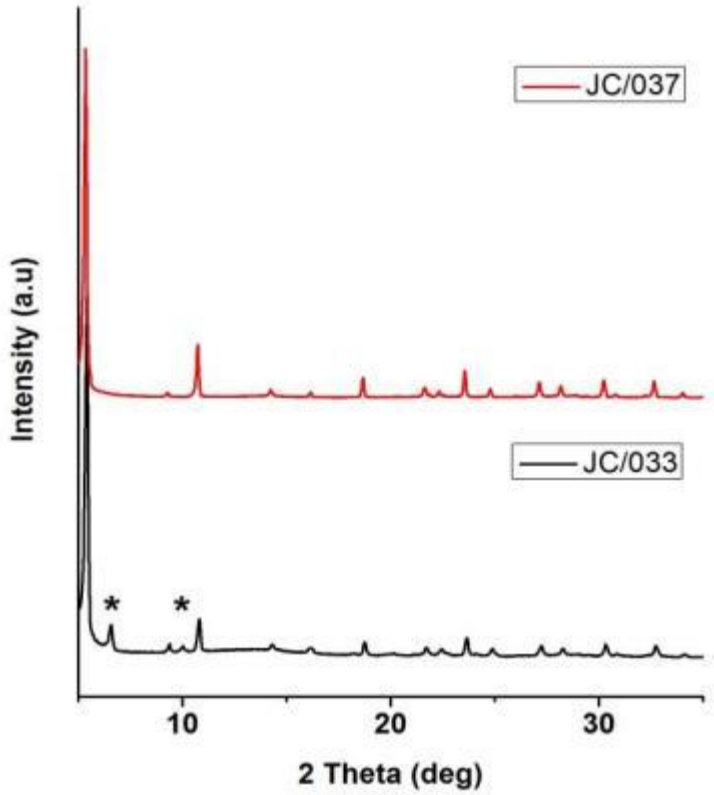

Figure 23 – Stacked XRD patterns of VPI-5 dehydrated under high vacuum at room temperature for 6 hours (black) and 24 hours freeze drying before 4 hours under vacuum at room temperature (red). Asterisks denote $AlPO_4$-8 impurities

This result presented freeze drying as a viable option for drying unstable microporous templates. However, as previously mentioned, this only proves phase retention rather than quantifying the amount of water lost. In future work it would be interesting to weigh a vial pre and post drying of a significant quantity of VPI-5 to assess the amount of water lost without any structural collapse.

Potentially, even without removal of chemisorbed water from VPI-5 it could still be viable as a moisture sensitive template. Due to the strength of the interaction of chemisorbed water with $Al(O)_4$ units it would not be surprising if it was unreactive to SCFED precursors. Moreover, freeze drying presents a simple method of drying templates.

Unfortunately, even after successfully isolating a freeze dried crystal in oil in an attempt to obtain a single crystal diffraction pattern, the cryostream (N_2 at 100 K) contained moisture and subsequently formed ice crystals on the sample. This manifested itself as solid

diffraction rings which were clearly more visible the longer the collection ran. The purpose of obtaining a single crystal image of a freeze dried sample was to compare to the fully hydrated single crystal pattern, as shown in section 3.1.5, to observe whether reduction in cell symmetry is comparable to that of $P6_3 \rightarrow C_m$ discussed previously in literature examples of dehydrated VPI-5. By disregarding the contaminated images, the pattern was able to be refined using the C_m group but no discernible structure could be obtained.

3.1.3 – Growth of Larger, Thicker VPI-5 Crystals

Due to the nature of VPI-5 growth, an inherent problem with mounting crystals onto a microelectrode arises from the relatively small dimensions of synthesised crystals, which lead to consideration as to how to increase both crystal length and thickness for subsequent ease of handling and mounting by a variety of different methods.

Following on from JC/028, there is logic to the idea that keeping a lower temperature crystallisation for a longer period of time would in theory continuously redissolve unreacted material to grow onto existing individual needles. Unfortunately a 7 day reaction at 125 ^{0}C resulted in a dense powder containing a large range of zeolitic products in which no VPI-5 crystals could be identified. Potentially, using an oven which can rotate autoclaves would continually mix the gel and perhaps be able to react for 7 days without all powder agglomerating.

It was also attempted to grow crystals from a flat substrate, potentially providing a nucleation site from which VPI-5 would grow in parallel bundles. Other attempts used a variety of substrates from amorphous/crystalline SiO_2, Al plate and Si plate, none of which showed any significant improvement. A potential solution could be the use of steam assisted growth of a substrate coated in VPI-5 precursor gel using a similar procedure described in section 2.2.

The next logical step was to attempt seeding growth using existing VPI-5 samples. 700 mg (roughly 10 % of a normal crystal yield) of VPI-5 grown at 135 ^{o}C was taken, broken into smaller fragments, and using the crystals as seeds in a 125 ^{o}C reaction to improve VPI-5 yield as larger needles.

Results were mixed, as the yield of impurity phase $AlPO_4$-H2 (of the $AlPO_4$-C structure) increased, yet the VPI-5 crystals recovered seemed different in morphology to the initial seeds put in. An increase in impurity is possibly due to the fact that single crystal growth is promoted by solution homogeneity, which the addition of solid seed crystals disrupts. So, whilst it provides a template for VPI-5 to grow onto, it also provides a wealth of nucleation sites for the crystallisation of smaller pore $AlPO_4$ species. Figures 24 and 25 show the templating crystals and the seeded growth crystals respectively.

Figure 24 – JC/025b crystal, scale is 200 µm

Figure 25 – JC/042 seeded crystal, scale is 200 µm

The crystals not only appeared to be larger but also clustered in more parallel bundles, as opposed to the cone shape adopted by the seed crystals. Logic dictated that the next step was to reseed again with 700 mg of JC/042. Although a few ~500 µm crystals were observed, denoting success, this was not seen as a basis for full confidence in the seeding

process as there was not a significant increase in overall crystal size by inspection. It was postulated that the large amount of crystalline $AlPO_4$-H2 in JC/042 was attributing to seeding of further growth of itself, much as the VPI-5 seeds had.

Efforts repeating seeded growth, but using 125 ^{o}C crystallised VPI-5 in the same manner, did not yield any different results. Again, as the crystals grown at 125 ^{o}C consisted of ~90 % impurity phases, it essentially ended up seeding more impurity phases.

From the results obtained there were promising signs for seeding growth of VPI-5, however impurities obtained at 125 ^{o}C crystallisations became problematic in future seeding attempts. A method was needed to reliably separate VPI-5 from other $AlPO_4$ impurities, leading into the following work of section 3.1.4.

3.1.4 – Separation Techniques

Samples of JC/042 were placed into solutions of glycerol to assess if VPI-5 clusters sank at different rates to impurity phases. Figures 26 and 27 show the optical microscopy images with the mild level of success using this technique, VPI-5 clusters tended to sink at a faster rate whereas needles tended to float. Impurity phases however did not seem to separate noticeably.

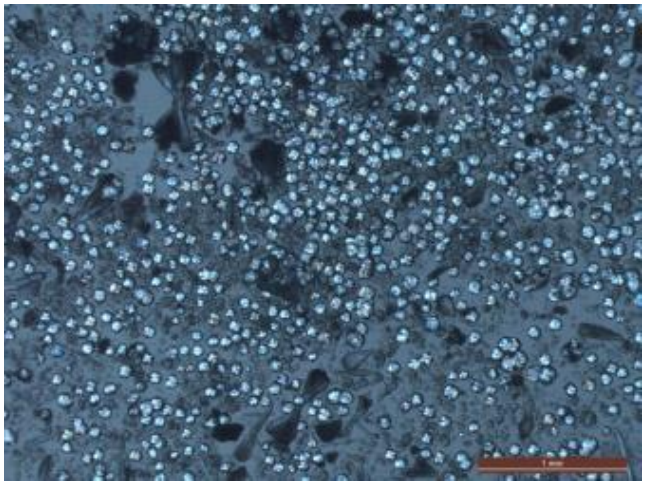

Figure 26 – Optical microscope image showing bottom fraction of glycerol separated VPI-5 crystals

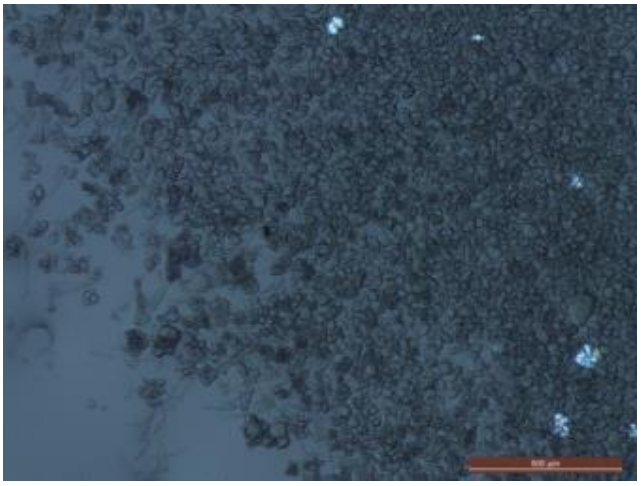

Figure 27 – Optical microscope image showing top fraction of glycerol separated VPI-5 crystals

As discussed previously, VPI-5 is approximately ~25 % water by mass due to its large hydrophilic pores and as such is likely to be, on average, less dense than other non-hydrated $AlPO_4$ impurities. Separation using a solvent which has a density between 2-3 g ml^{-1} that would not displace pore water in VPI-5 was desirable.

Chloroform, with a density of 1.48 g ml^{-1}, is miscible in bromoform, which has a density of 2.89 g ml^{-1}. Neither solvent has a particular affinity for water, so by control of solvent composition it was hoped that VPI-5 and $AlPO_4$-H2 (alongside other impurities) could be separated. Figure 28 below shows that a solution of 35 % bromoform in chloroform demonstrated the best separation capabilities.

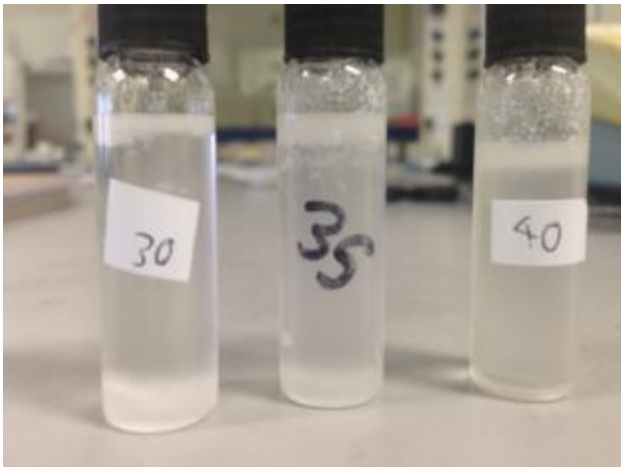

Figure 28 – Solutions of bromoform/chloroform with JC/042 crystals, labelled as % bromoform content

Isolating crystals from the top and bottom layers and observing under an optical microscope is depicted in figures 29 and 30.

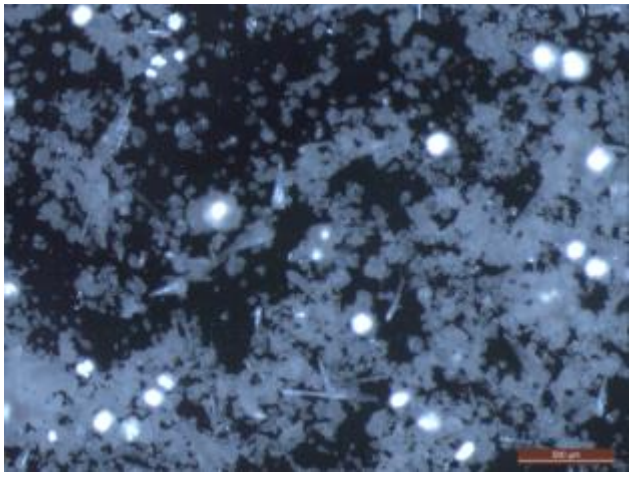

Figure 29 - JC/042 separations in 35 % bromoform showing the bottom fraction, scale is 500 µm

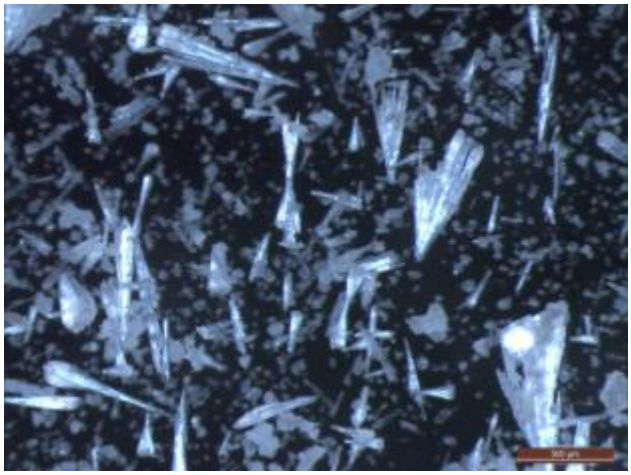

Figure 30 – JC/042 separations in 35 % bromoform showing the top fraction, scale is 500 µm

As predicted, VPI-5 crystals clearly float whilst unwanted impurity phases sink. Due to both phases binding to one another to some extent, a truly perfect separation of material is not feasible. However this mixture of chloroform/bromoform clearly was effective.

Separations on a larger scale proved difficult, with volatility of large amounts of chloroform and breaking up clumps of crystals and, due to the amount of JC/042 powder used previously, only 300 mg of pure JC/042 VPI-5 crystals were obtained to seed with. A gel was seeded with this 300 mg of VPI-5 crystals yet did not produce the expected improvement in

crystal yield nor size. Future work should centre on repeating the process from scratch to obtain ~1000 mg of first generation seeded pure VPI-5 (isolated JC/042) for seeding further reactions, however time constraints prevented this.

Figure 31 shows stacked XRD plots of: JC/025b – pure VPI-5 clusters grown at 135 ^{o}C, JC/028 – predominantly amorphous material with some VPI-5 needles, JC/042 – seeded growth at 125 ^{o}C with 700 mg JC/025b producing more crystalline impurity yet better VPI-5 crystals, and finally JC/045 – seeded growth at 125 ^{o}C using 300 mg of separated JC/042.

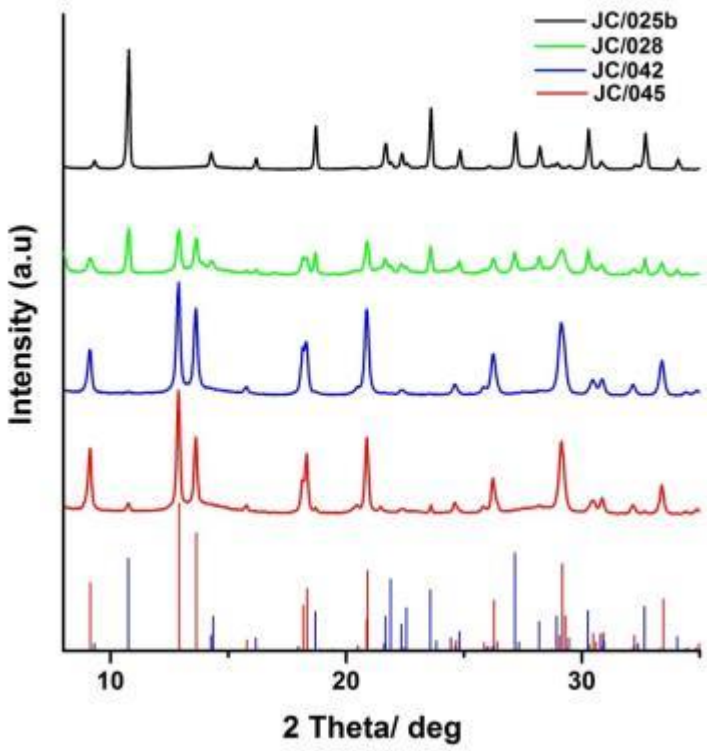

Figure 31 – Stacked XRD plots of VPI-5 synthesis attempts, with expected reflections for VPI-5 (red) and $AlPO_4$-H2 which adopts the $AlPO_4$-C structure (blue)

Perhaps the use of too few crystals has an adverse effect on seeded growth, further attempts using a higher quantity of pure seed crystals, grown at 125 ^{o}C, will be explored. There is also scope to simply use JC/025b seed crystals and grow at 135 ^{o}C to observe any further possible growth.

3.1.5 – Framework Substitution

The unusual hydrophilic nature of the pores of VPI-5, in contrast to several other aluminophosphates, can be attributed to the aforementioned chemisorbed water necessitated for the strained AlO_4 units, formed at cis-D4R junctions, to adopt a desired octahedral geometry. Removal of this water under atmospheric conditions induces structural instability and inevitable collapse to $AlPO_4$-8.

Figure 32 below is a refined single crystal diffraction pattern obtained from a needle of JC/028, the highlighted spheres in the centre of the pores denotes unassigned oxygen atoms from physisorbed water. Note the assigned oxygen atoms pointing into the pores are from chemisorbed water molecules.

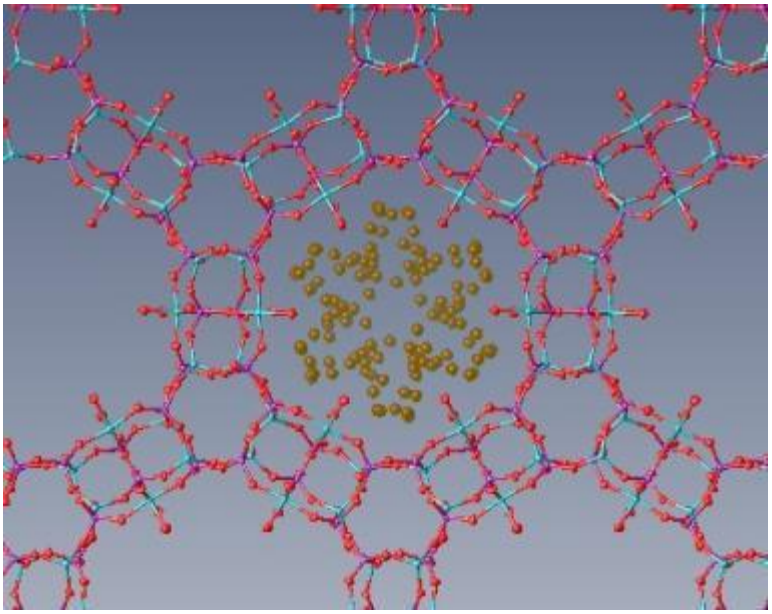

Parameter	Value	Parameter	Value
a	18.945(4)	**α**	90
b	18.945(4)	**β**	90
c	8.026(2)	**γ**	120
Z'	4	**R1**	11.58 %*

Figure 32/ Table 3 – JC/028 single crystal diffraction pattern, collected as symmetry group $P6_3$/ Corresponding refined crystal structure parameters.

It should also be noted that not assigning the unbound water molecules in the centre of the pore prevented any further reduction in the value of R1.

Substitution of the chemisorbed water of $AlO_4(H_2O)_2$ units with a chelating bidentate ligand might stabilise the structure whilst removing pore water and active groups. Ethylene glycol ($HOCH_2CH_2OH$) has potential to form a 5-membered ring with Al in the desired geometry replacing chemisorbed water molecules. Both oxygen atoms in ethylene glycol could act as donors in the same manner as the displaced water atoms. Moreover, as ethylene glycol has a boiling point of 196-198 ^{o}C it would, in theory, not suffer from the same thermal instability above 100 ^{o}C compared to chemisorbed water substituents. In addition to this the bidentate binding of a glycol ligand could be stronger than that of 2 separate ligands.

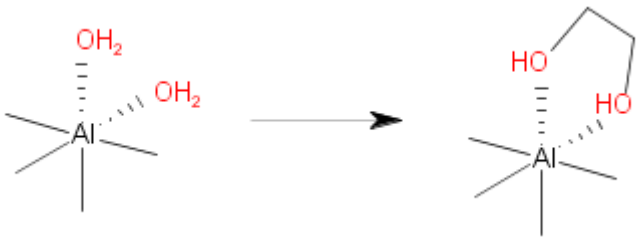

Figure 33 – Proposed substitution of chemisorbed water with ethylene glycol

The drying agent to be used for removal of water from VPI-5 was BaO, the quantity of which to be used was calculated as below:

$$Formula\ weight\ (VPI-5,\ Al_3P_3O_{12}.7H_2O) = 491.85 g\ mol^{-1}$$

$$Formula\ weight\ (7H_2O) = 126\ g\ mol^{-1}$$

$$\%\ Weight\ as\ water = \frac{126.00}{491.85}\ x\ 100 = \mathbf{25.6}\ \%$$

Given that 0.1 g of water is dried by 1.0 g BaO, as per literature, the quantity of BaO would be calculated as:

$$Quanity\ (BaO) = Weight\ (VPI-5)\ x\ 2.56$$

This would factor in for multiplying by 0.256 for the fraction of VPI-5 that is water and the 10:1 ratio of BaO:Water. It should also be noted that excess BaO was to be used as there could be water present in glassware and ethylene glycol, albeit minimal.

500 mg of JC/026 was placed in a cellulose thimble. Separately, a 125 ml Teflon liner was charged with ethylene glycol (15 ml) and barium oxide (2.562 g, 16.7 mmol). The thimble

was placed upon 2 magnetic stirrer bars to space the thimble from the powder, and the liner placed in an autoclave and heated to 210 ^{o}C for 24 hours. Unfortunately, as was anticipated, the cellulose thimble did not survive the reaction conditions and as such the powder was not recoverable.

As temperatures past 100 ^{o}C were desired, but solvothermal means were not viable, a refluxing experiment was carried out. Ethylene glycol was dried over sodium, producing a significant amount of heat upon forming sodium alkoxide product, and refluxed at ~200 ^{o}C for 8 hours in Soxhlet apparatus whereby hot solvent washed through a cellulose thimble containing 500 mg JC/026 VPI-5 crystals. These crystals were recoverable however upon XRD analysis some degradation to $AlPO_4$-8 was observed with no improved thermal stability.

Perhaps the size of an Al atom does not permit formation of the desired 5 membered ring. As propylene glycol has a comparable boiling point to ethylene glycol, but evidently would form a 6 membered ring, it could be an interesting future experiment.

3.2 - Silicalite-1 (SL-1)

Another interesting prospect is the growth of a zeolitic thin film. In the literature the Al/Si precursors are deposited by hot wall CVD onto a conductive substrate, then the templating agent dip coated onto it. Hydrothermal conditions then promote the growth of a dense zeolitic film on the substrate with no macroscopic cracks. [44]

This potentially could be a very easy way to mount crystalline templates onto an electrode, however a few issues remain. The gaps between crystallites would be significantly larger than the micropores, so deposition would occur between crystal gaps. Moreover, the direction of crystal growth from the electrode would be difficult to control.

For the purpose of supercritical fluid electrodeposition, a film would be grown onto a TiN surface. For the substrates we used, SiO_2 is deposited on the TiN/Si substrates by sputtering, they are then coated with polymethylmethacrylate (PMMA), to protect the surface from dust build up during cutting, before cutting into 1 x 1 cm^2 samples. Substrates in the literature were washed with deionised water and acetone to remove the PMMA and generally clean the surface.

Our thoughts were that we could opt for harsh cleaning conditions to ensure the substrate was suitable for use. Piranha solution, known as Caro's acid or H_2SO_5, is produced from a mixture of 3.75 ml sulphuric acid (98 %) with 1.25 ml H_2O_2 (>30 wt %) which is highly corrosive and a strong oxidiser of organics. Experiments were performed using different levels of cleaning, from control samples with no cleaning whatsoever to varying lengths of times.

As previously discussed in section 1.4, there are 2 setups which the literature paper performed these film growths, vapour phase transport (VPT) or steam assisted crystallisation (SAC). Both techniques require the substrate to be raised out of the solution on a Teflon stand; however in SAC the template is directly applied to the substrate before synthesis whereas in VPT it is combined with water at the bottom of the autoclave. VPT is more liable to convert the Si part of the substrate to zeolite as well as the SiO_2 surface.

The Teflon inserts used in the literature were hand-made, and after a collaborative visit to UCL we had similar apparatus made for our larger volume autoclaves. Figure 34 shows our

Teflon stand, with perforated discs to allow vapour transport to the substrate. The disc with a central hole is used for VPT as the substrate faces downwards.

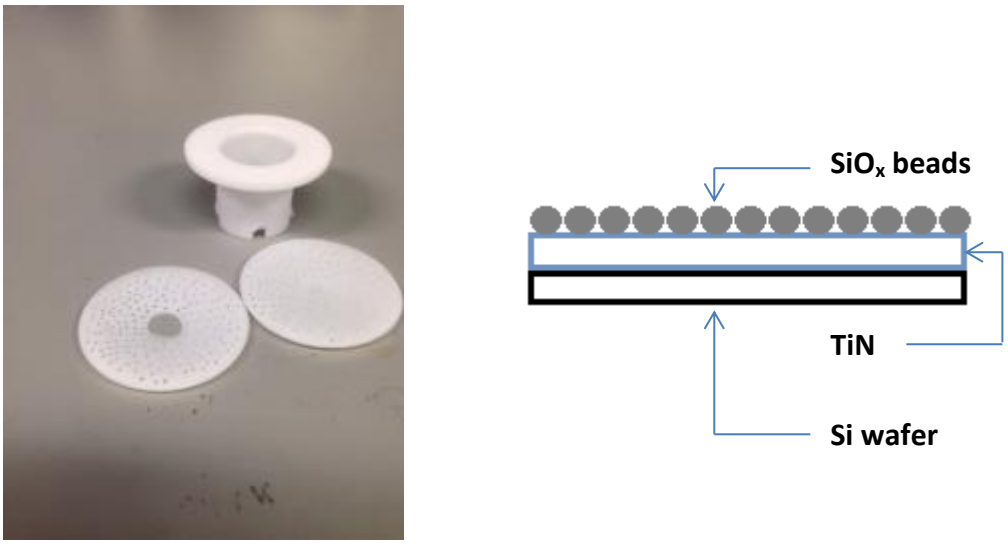

Figure 34 – Left: Teflon insert (top) with 2 perforated discs for SAC (lower right) and VPT (lower left), Right: SiO_x/TiN/Si substrate, TPAOH is applied directly to the surface of the beads

Figure 35 shows 3 separate SiO_2/TiN/Si substrates coated on the SiO_2 face in tetrapropylammonium hydroxide (TPAOH) in a 125 ml autoclave, with 14 ml of water underneath in a SAC setup.

Figure 35 – 3 substrates, each cleaned in different manners, coated in TPAOH ready for SAC

One control sample was not cleaned whereas the 2 others were placed in piranha solution for 10 and 30 minutes respectively. After coating with TPAOH and setup with SAC apparatus using 14 ml H_2O they were crystallised for 48 hours at 180 ^{o}C. This was a standard procedure followed from the literature; however, a major amount of Si substrate was also converted during the process made evident by formation of white crystallites on the bottom of the substrate.

Grazing incidence XRD collected at a 0.2 ^{o} incident angle of the uncalcined samples, top SiO_2 facing, did show reflections which could be assigned to SL-1 growth. However, as a vast majority of the samples showed incomplete, patchy film growth not a lot of useful information could be ascertained from the XRD patterns. To be able to compare to the literature [44], visual inspection of the films by SEM proved to be a much more useful and insightful technique.

The following 3 samples used the same set of cleaning procedures (none, 10 min, 30 min) as previous and using the same quantity of water, however the crystallisation process was performed at 130 ^{o}C for only 24 hours as opposed to the previously longer reaction time. Less white crystallites were observed across the whole substrate which alongside less observed corrosion of the Si substrate denoted less conversion of Si in comparison to SiO_2 than at 180 ^{o}C for 48 hours.

Calcination at 550 ^{o}C in air for 3 hours turned all of the above samples to a dark shade of purple from a previous gold colour.

It was postulated that degradation of the downward facing Si part of the substrate could be due to too high a quantity of water being used. A repeat of the reaction was performed using no piranha cleaning and crystallising at 130 ^{o}C for 24 hours, but with 7.0 ml and 3.5 ml of water respectively. Using 7.0 ml of water produced a noticeably more evenly covered and less reflective film by comparison, whereas using 3.5 ml of water showed a multi-coloured reflective surface. In both cases less Si degradation was observed comparatively, scaling inversely with quantity of water used. A repeat experiment using 3.5 ml of water was performed, but crystallising at a higher temperature of 180 ^{o}C for 24 hours.

Time constraints limited further experiments; however, SEM images were obtained for different samples which gave a better insight to the effects of cleaning, quantity of water and crystallisation conditions as demonstrated by the following figures. All of the following samples were obtained from samples calcined at 550 ^{o}C in air and then sputtered with gold to improve image resolution by FEG-SEM.

The film grown at 130 ^{o}C for 24 hours showed inconsistent growth and upon further inspection it was clear that a particular spot in the SiO_2 surface had been penetrated and film growth had spanned from there.

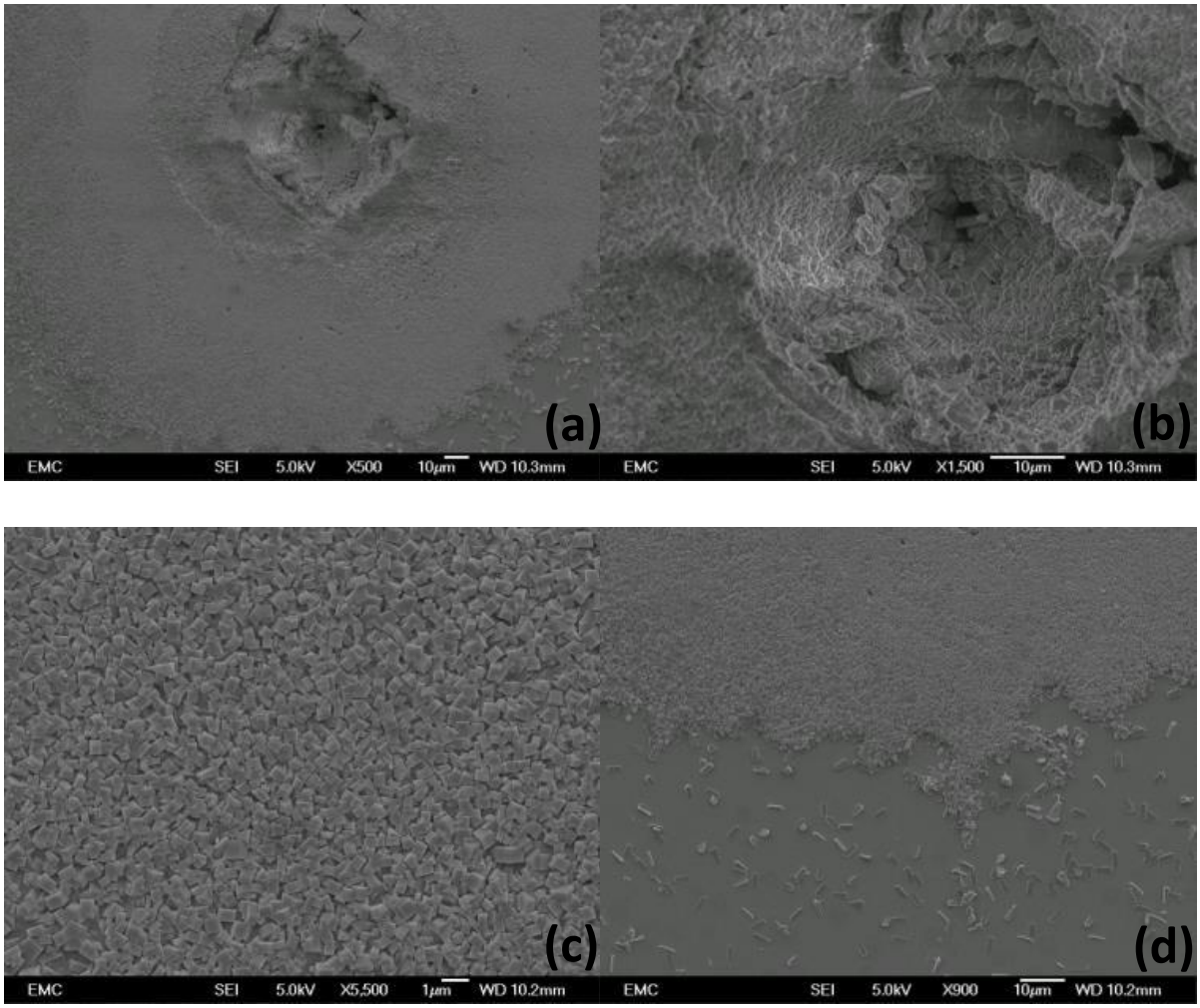

Figures 36 a-e – SEM images of a calcined SL-1 film grown at 130 ^{o}C for 24 hours on TiN/Si (JC/056)

Figure 36 b shows that the film has grown into the substrate and nucleated from there. Interestingly figure 36 c shows that from the edge of the hole in the substrate outwards film

growth is even with several overlaying crystals forming a similar film to that described in literature. The individual crystals however, shown on the periphery of figure 36 d and close up in 36 e, clearly are of the coffin shape SL-1 crystals depicted in figure 13.

The film grown under the exact same crystallisation conditions but with the addition of a 30 minute piranha solution pre-treatment demonstrated a significant difference in film growth and crystal shape.

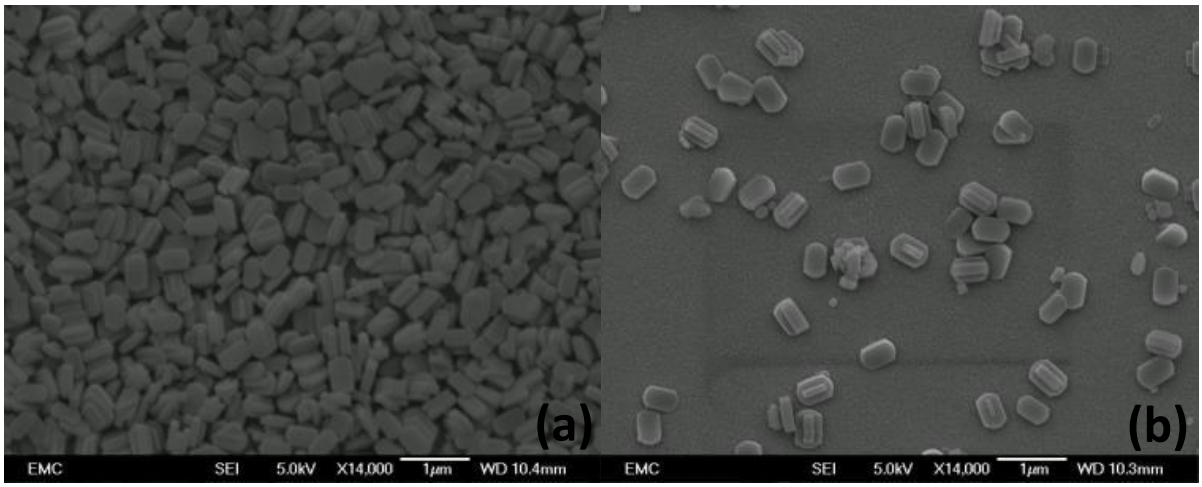

Figures 37 a-b – SEM images of a pre-treated calcined SL-1 film grown at 130 ^{o}C for 24 hours on TiN/Si (JC/058)

By adjustment of only pre-treatment of the substrate and keeping identical reaction conditions the leaflet shaped crystal can be obtained instead, characterised by oval shape and perpendicular growth of additional crystals. However the film did not appear to be interlaced in the same manner as figure 36 c but rather individual crystallites layered on top of one another.

Further evidence to the degree of control that be exerted over the resulting morphology by changing a singular variable is demonstrated figures 38 a-b. This was the film again grown at 130 ^{o}C for 24 hours but using 7.0 ml instead of 14.0 ml of water.

Film growth was uniform across the whole substrate, significantly less Si was degraded and the texture of the film changed noticeable. Figure 38a illustrates that even down to a 1 μm level there is defined texture to the individual crystallites. The film appeared to be consisted of heavily intergrown “leaflet shaped” crystals forming pseudo-spherical clusters.

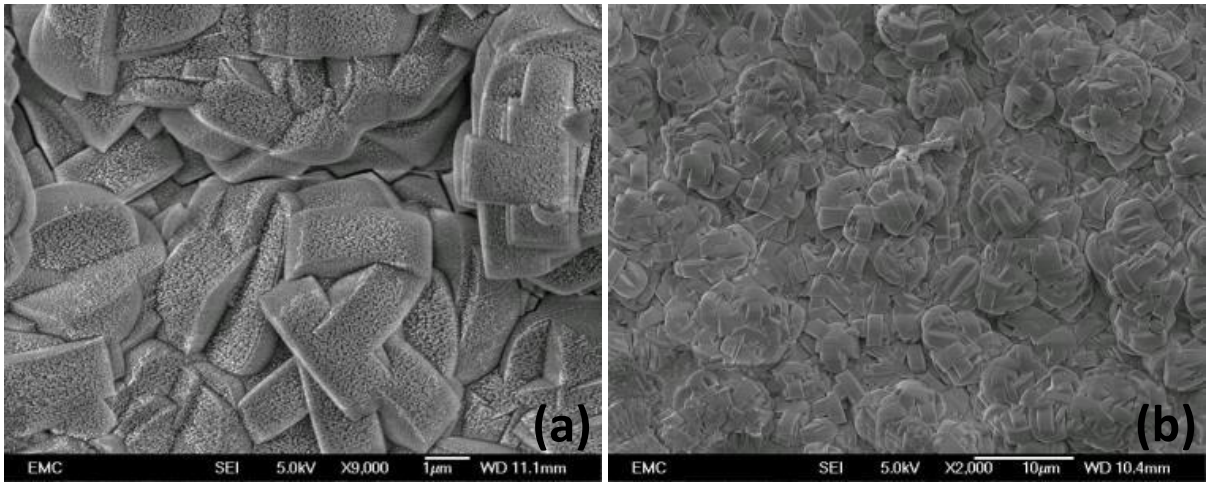

Figures 38 a-b – SEM images of a calcined SL-1 film grown at 130 ^{o}C for 24 hours on TiN/Si using 7.0 ml of water (JC/061)

Again due to time constraints no further work was performed on SL-1 films, specifically the lack of results with films gown at 180 ^{o}C, however it was extremely interesting to observe the level of control that could be achieved by altering substrates and crystallisation slightly. More work to achieve repeat results is needed, and more variables changed to assess their true effect on film growth. Despite this, the initial work on these templates has been promising and is a good step forward for this area of the project.

3.3 – Grafting into Anodic Alumina (AAO) Membranes

3.3.1 – Template Modification

As some metal precursors can be particularly sensitive to moisture, i.e. germanium, it can be useful to have a template which is not only easier to dry but is less susceptible to absorbing moisture in the first instance.

Anodic alumina is notably hygroscopic due to its surface being lined with hydroxyl groups. By using the strong aluminophosphate linkage, with an organic group tethered to the phosphorus, it is feasible to invert the hydrophilicity of these membranes.

Diethylphenylphosphonate, shown in figure 39, was synthesised from phenylphosphonic dichloride and ethanol in a highly exothermic condensation reaction. The purity of the starting material was ~90 % and an excess was used to act as a drying agent for ethanol. Any moisture converts the dichloride to phenylphosphonic acid, which can still graft and is not a problematic impurity.

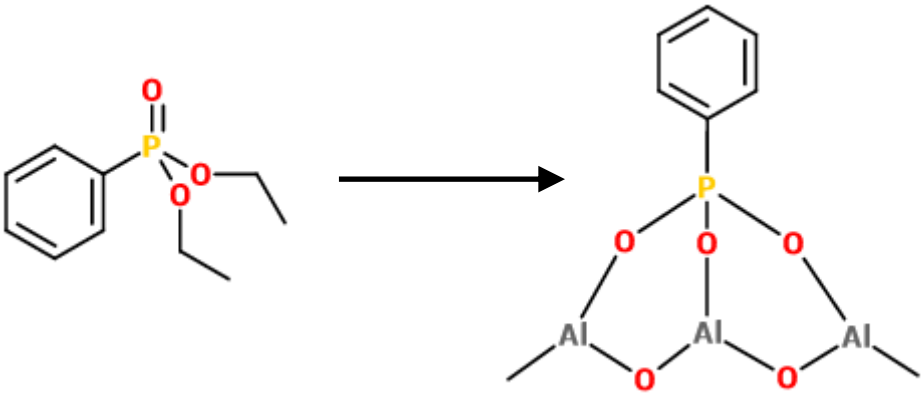

Figure 39 – Postulated method of phosphonate grafting onto alumina, note that the tetravalent phosphorus is suggested to possess an additional delocalised bond shared between the 3 P-O linkages

The literature stated that the grafting was performed with 1 g powdered Al_2O_3 with 40 ml of dichloromethane (DCM) solvent and a 5 fold excess of grafting agent, relative to the proposed quantity of phosphonate required to cover the entire area of alumina. AAO membranes weigh approximately 100 mg each (sometimes several were used in the same reaction), however scaling down the reaction tenfold would be have been impractical. As such, the same quantities of grafting agent and solvent were used as stated above, keeping the concentration of the solution identical but providing a large excess in grafting agent.

An issue with the mixing soon became apparent as in the literature alumina powder is simply stirred whilst refluxing at 40 ^{o}C. AAO membranes are notably fragile, so mixing would have to be carried out via reflux. However, at 40 ^{o}C refluxing is gentle so more potent conditions were employed via a reflux at 75 ^{o}C, evidently DCM boils past 40 ^{o}C however the higher temperature ensured the entire solution was vigorously refluxing as opposed to a small fraction.

An attempt was made to graft phosphonate groups in 200 nm pore AAO, and dropping water onto the dried membrane resulted in the lack of absorption shown in figure 40.

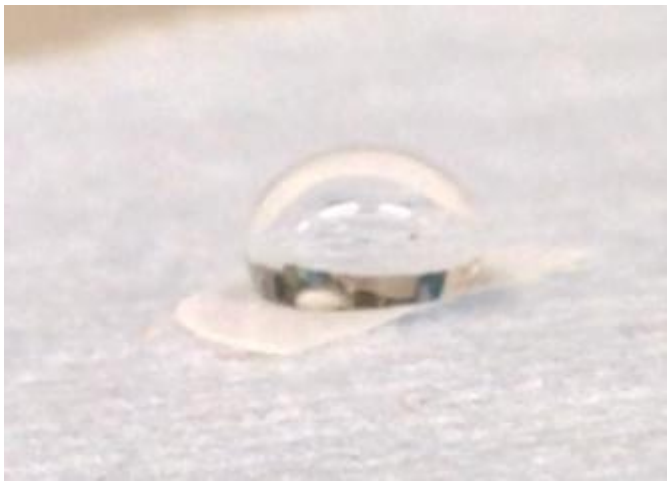

Figure 40 – Water droplet upon phosphonate grafted 200 nm AAO

An unmodified 200 nm AAO membrane readily absorbs water and would let it pass through to the tissue. Figure 40 demonstrates that post grafting there is a large reluctance for the membrane to absorb water. The hydrophobicity exhibited is likely to be largely from the membrane surface, however given the large size of the pores (relative to a water molecule) it does suggest that the pore walls inside the membrane have been grafted as surface hydrophobicity alone would not be sufficient to prevent absorbtion of water.

For use as a deposition template, the membrane would have to be contacted with a gold/chromium alloy. The membranes were particularly fragile to handle for the grafting process, and as such contacting with gold prior to this would reduce the chance of the membrane fracturing. However, permeation of grafting agent into the pores of a membrane which is blocked from one face could also present problems with sufficient grafting.

Using 13 nm pore AAO, 2 membranes were first grafted before attempting to contact with gold/chromium, conversely grafting into a pre-contacted 13 nm membrane was also attempted. It was clear that contacting prior to grafting was not a viable option and as such all following membranes were contacted post grafting.

Note that, for the following experiments, grafting time was reduced from 48 hours to 24 to see whether any detriment was noticed with respect to grafting. Both 13 nm and 55 nm pore AAO membranes were used in these 24 hour reactions.

Both the 13 and 55 nm pore membranes showed similar behaviour to the 200 nm AAO membranes, forming a large unabsorbed water droplet as in figure 40 previously and showing no difference to 48 hour grafted samples. In addition to testing the absorption of water, the absorption of dichloromethane (DCM) was also tested. With an unaltered AAO membrane DCM sits on the surface until evaporation; however, with both the 13 and 55 nm pore grafted AAO there was evidence of absorption. The membranes became significantly more fragile by comparison and frequently split when handled with tweezers.

The prevention of water absorption post grafting suggested a level of hydrophobicity was introduced to the membranes, however to quantify the improvement on their intended use as SCFED templates further experimentation was required.

3.3.2 – Attempts at SCFED into Modified AAO Membranes

Prior to deposition attempts, templates were contacted with an epoxy resin ready for the SCFED process. These templates were then dried at 120 ^{o}C under vacuum and transferred directly to a glovebox to ensure the templates were as dry as possible.

The 13 and 55 nm pore templates were used for the attempted SCFED of germanium, however after FEG-SEM cross-sectional EDS analysis no Ge signal was observed along the pores of either template. So, despite evidence of increased hydrophobicity of the templates, it did not improve upon the problematic SCFED of Ge. Future work comparing the SCFED of tellurium, a much more reliable deposition, between grafted and non-grafted membranes would be a good starting point to observe differences in deposited material. Perhaps with attempting Ge deposition so soon we were attempting too many steps at once.

4 – Conclusions and Further Work

4.1 – VPI-5

Single crystal growth was successfully replicated from literature work, being able to produce both individual needles and clusters of VPI-5. Freeze drying of single crystals has proven to be a viable means of removing water from VPI-5 without causing any structural collapse to $AlPO_4$-8.

A simple test to assess the level of dehydration achieved would be to weigh a sample of VPI-5 before and after freeze drying. In tandem, thermogravimetric analysis (TGA) would hopefully show the separate "types" of physisorbed and chemisorbed water being removed and quantify the amount lost at each stage. Dividing the mass lost by the calculated total mass of water in VPI-5 would give an indication as to the extent of dehydration achieved by freeze drying.

Unfortunately, not many significant steps were taken in the direction of mounting crystals for use as electrodes, due to some time constraints and other priorities. The current largest size crystals were approximately ~0.5 mm in length, which although is considered large as a zeolite crystal, does still present significant challenges in mounting. Potentially, seeded growth could be experimented with further to attempt to grow even larger crystals.

The work on framework substitution is an interesting topic as VPI-5 has historically been characterised as an unstable material due to the necessity of framework bound water, whereas many aluminophosphate catalysed reactions require temperatures which would degrade VPI-5. In theory, there is no reason as to why a bidentate alkane diol could not take the place of the 2 cis arranged bound water molecules surrounding Al units in the pores. In addition to this, the presence of alkyl chains instead of just exposed OH groups could change the properties of the pores themselves.

4.2 – SL-1

The work from the literature has successfully been replicated using a new substrate, TiN, a significantly larger autoclave and coating SiO_2 by sputtering instead of hot wall CVD. This demonstrates that the versatility of the technique has been tested even further. Sample JC/061 in particular showed very similar results to literature samples despite the differences

in conditions. Furthermore, by changing very few conditions, the morphology of the resulting SL-1 film was demonstrably different, suggesting a high level of control could be possible.

The primary reason for this line of work was to eventually pursue oriented films, which do exist in the literature. If our work on randomly oriented films were to be successful to the extent of complete film coverage, a clear next step would be to synthesise SL-1 seed crystals for use in growing oriented SL-1 films. Further to this, work could be pursued to make larger pore aluminosilicates/aluminophosphates.

An inherent problem with oriented films, discussed previously, arises from the thickness of the synthesised film. Etching this film down to a workable aspect ratio could be time consuming and unreliable.

4.3 – AAO

Extremely good progress has been made on alteration of the hydrophilic nature of anodic alumina membranes as evidenced by contact angle measurements and dichloromethane absorption.

The procedure to synthesise the grafting agent is not a perfect one. By using a 90 % pure starting material, it incurs impurities from the start, yet the impurities themselves should not be problematic as the hydrated forms can also acts as grafting agents. This route was taken as ordering pure grafting agent came with a lengthy delivery time. However, to provide the best conditions for grafting a pure reagent would be the most ideal.

As Ge deposition into grafted templates has not been successful, steps to assess the difference in properties between the grafted and non-grafted membranes should be tested with a more robust deposition element such as Te.

In addition to this the extent of grafting needs to be assessed past simple contact angle measurements. TGA would once more be a helpful method of assessing levels of moisture in grafted and ungrafted membranes. As it stands the membranes are currently being analysed by fracturing and performing cross-sectional FEG-SEM EDS in the same manner that electrodeposition is assessed. Hopefully strong phosphorus signals will be seen consistently along the pores throughout the membranes.

5 – Appendix

5.1 – Bibliography

(1) Ke, J.; Su, W.; Howdle, S. M.; George, M. W.; Cook, D.; Perdjon-Abel, M.; Bartlett, P. N.; Zhang, W.; Cheng, F.; Levason, W.; Reid, G.; Hyde, J.; Wilson, J.; Smith, D. C.; Mallik, K.; Sazio, P. *Proc. Natl. Acad. Sci. U. S. A.* **2009**, *106*, 14768–14772.

(2) Cook, D.; Bartlett, P. N.; Zhang, W.; Levason, W.; Reid, G.; Ke, J.; Su, W.; George, M. W.; Wilson, J.; Smith, D.; Mallik, K.; Barrett, E.; Sazio, P. *Phys. Chem. Chem. Phys.* **2010**, *12*, 11744–11752.

(3) Bartlett, P. N.; Cook, D. C.; George, M. W.; Ke, J.; Levason, W.; Reid, G.; Su, W.; Zhang, W. *Phys. Chem. Chem. Phys.* **2010**, *12*, 492–501.

(4) Ke, J.; Bartlett, P. N.; Cook, D.; Easun, T. L.; George, M. W.; Levason, W.; Reid, G.; Smith, D.; Su, W.; Zhang, W. *Phys. Chem. Chem. Phys.* **2012**, *14*, 1517–1528.

(5) Bartlett, P. N.; Cook, D. a; George, M. W.; Hector, a L.; Ke, J.; Levason, W.; Reid, G.; Smith, D. C.; Zhang, W. *Phys. Chem. Chem. Phys.* **2014**.

(6) Bartlett, P. N.; Cook, D. C.; George, M. W.; Ke, J.; Levason, W.; Reid, G.; Su, W.; Zhang, W. *Phys. Chem. Chem. Phys.* **2011**, *13*, 190–198.

(7) Jiang, J.; Jorda, J. L.; Diaz-Cabanas, M. J.; Yu, J.; Corma, A. *Angew. Chem. Int. Ed. Engl.* **2010**, *49*, 4986–4988.

(8) Corma, a; Díaz-Cabañas, M. J.; Jiang, J.; Afeworki, M.; Dorset, D. L.; Soled, S. L.; Strohmaier, K. G. *Proc. Natl. Acad. Sci. U. S. A.* **2010**, *107*, 13997–14002.

(9) Schaefer, H.-E. *Nanoscience: The Science of the Small in Physics, Engineering, Chemistry, Biology and Medicine*; Springer Science & Business Media, 2010.

(10) Davis, R. *International Assessment of Research and Development in Catalysis by Nanostructured Materials*; Imperial College Press, 2011.

(11) McCusker, L. B.; Liebau, F.; Englehardt, G. *Microporous Mesoporous Mater.* **2003**, *58*, 3–13.

(12) Liu, L.; Yu, Z.-B.; Chen, H.; Deng, Y.; Lee, B.-L.; Sun, J. *Cryst. Growth Des.* **2013**, *13*, 4168–4171.

(13) Corma, A.; Díaz-Cabañas, M. J.; Jordá, J. L.; Martínez, C.; Moliner, M. *Nature* **2006**, *443*, 842–845.

(14) Cejka, J.; Corma, A.; Zones, S. *Zeolites and Catalysis: Synthesis, Reactions and Applications*; Wiley, 2010.

(15) Sun, J.; Bonneau, C.; Cantín, A.; Corma, A.; Díaz-Cabañas, M. J.; Moliner, M.; Zhang, D.; Li, M.; Zou, X. *Nature* **2009**, *458*, 1154–1157.

(16) Strohmaier, K. G.; Vaughan, D. E. W. *J. Am. Chem. Soc.* **2003**, *125*, 16035–16039.

(17) Lobo, R.; Tsapatsis, M. *J. Am. Chem. Soc.* **1997**, *7863*, 8474–8484.

(18) Jiang, J.; Jorda, J. L.; Yu, J.; Baumes, L. a; Mugnaioli, E.; Diaz-Cabanas, M. J.; Kolb, U.; Corma, A. *Science* **2011**, *333*, 1131–1134.

(19) Karlsson, A.; Akporiaye, D.; Stöcker, M. *Microporous Mater.* **1995**, *4*.

(20) Wu, Y.; Chmelka, B.; Pines, A.; Davis, M. *Nature* **1990**, *346*, 550–552.

(21) Martens, J.; Feijen, E. *J. Phys. Chem.* **1991**, *95*, 10025–10031.

(22) Man, A. De. *J. Phys. Chem.* **1992**, *10466*, 10460–10466.

(23) He, H.; Barr, T.; Klinowski, J. *J. Phys. Chem.* **1994**, *98*, 8775–8779.

(24) Venkatathri, N. *Bull. Mater. Sci.* **2003**, *26*, 279–281.

(25) Potvin, C.; Manoli, J. M.; Briend, M.; Barthomeuf, D. *Catal. Letters* **1991**, *10*, 225–232.

(26) Davis, M. E.; Saldarriaga, C.; Montes, C.; Garces, J.; Crowder, C. *Zeolites* **1988**, *8*, 362–366.

(27) Davis, M. E. *Nature* **2002**, *417*, 813–821.

(28) García-Carmona, J.; Fanovich, M. *Microporous Mesoporous Mater.* **2002**, *54*, 127–137.

(29) Sarı, U.; Kırındı, T.; Yüksel, M.; Ağan, S. *J. Alloys Compd.* **2009**, *476*, 160–163.

(30) Davis, M.; Montes, C. *J. Am. Chem. Soc.* **1989**, *111*, 3919–3924.

(31) Martínez, J. de O.; McCusker, L. .; Baerlocher, C. *Microporous Mesoporous Mater.* **2000**, *34*, 99–113.

(32) Anderson, J. R.; Jackson, W. R.; Hay, D.; Yang, Z.; Campi, E. M. *Zeolites* **1996**, *16*, 15–21.

(33) Sorby, K.; Szostak, R.; Ulan, J. G.; Gronsky, R. *Catal. Letters* **1990**, *6*, 209–214.

(34) Goldfarb, D.; Li, H.; Davis, M. E. *J. Am. Chem. Soc.* **1992**, 3690–3697.

(35) Cheetham, G.; Harding, M. *Zeolites* **1996**, *2449*, 3–6.

(36) Annen, M. J.; Young, D.; Davis, M. E.; Cavin, O. B.; Hubbard, C. R. *J. Phys. Chem.* **1991**, *95*, 1380–1383.

(37) De Oñate Martinez, J.; Falamaki, C.; Baerlocher, C.; McCusker, L. . *Microporous Mesoporous Mater.* **1999**, *28*, 261–269.

(38) Prasad, S.; Vetrivel, R. *J. Phys. Chem.* **1994**, *98*, 1579–1583.

(39) Davis, M.; Saldarriaga, C.; Montes, C. *Nature* **1988**, *25*, 698–699.

(40) Li, H.; Davis, M. E. *J. Chem. Soc. Faraday Trans.* **1993**, *89*, 957–964.

(41) Kim, H. S.; Lee, S. M.; Ha, K.; Jung, C.; Lee, Y.-J.; Chun, Y. S.; Kim, D.; Rhee, B. K.; Yoon, K. B. *J. Am. Chem. Soc.* **2004**, *126*, 673–682.

(42) Cao, T.; Pham, T.; Nguyen, T. H.; Yoon, K. B. *Angew. Chem. Int. Ed. Engl.* **2013**, *52*, 8693–8698.

(43) Zhou, M.; Korelskiy, D.; Ye, P.; Grahn, M.; Hedlund, J. *Angew. Chem. Int. Ed. Engl.* **2014**, *53*, 3492–3495.

(44) Bhachu, D. S.; Smith, A. J.; Parkin, I. P.; Dent, A. J.; Sankar, G. *J. Mater. Chem. A* **2013**, *1*, 1388–1393.

(45) Pham, T. C. T.; Kim, H. S.; Yoon, K. B. *Science* **2011**, *334*, 1533–1538.

(46) Wang, Z.; Yu, T.; Nian, P.; Zhang, Q.; Yao, J.; Li, S. *Langmuir* **2014**, *30*, 4531–4534.

(47) Ji, C.; Tian, Y.; Li, Y.; Lin, Y. S. *Microporous Mesoporous Mater.* **2014**, *186*, 80–83.

(48) Lee, T.; Choi, J.; Tsapatsis, M. *J. Memb. Sci.* **2013**, *436*, 79–89.

(49) Lee, J. S.; Kim, J. H.; Lee, Y. J.; Jeong, N. C.; Yoon, K. B. *Angew. Chem. Int. Ed. Engl.* **2007**, *46*, 3087–3090.

(50) Zhou, M.; Hedlund, J. *J. Mater. Chem.* **2012**, *22*, 3307.

(51) Zhang, B.; Zhou, M.; Liu, X. *Adv. Mater.* **2008**, *20*, 2183–2189.

(52) Yoon, K. B. *Acc. Chem. Res.* **2007**, *40*, 29–40.

(53) Cao, T.; Pham, T.; Nguyen, T. H.; Yoon, K. B. *Angew. Chem. Int. Ed. Engl.* **2013**.

(54) Li, F.; Zhang, L.; Metzger, R. *Chem. Mater.* **1998**, *4756*, 2470–2480.

(55) Villemin, D.; Moreau, B.; Siméon, F.; Maheut, G.; Fernandez, C.; Montouillout, V.; Caignaert, V.; Jaffrès, P.-A. *Chem. Commun.* **2001**, 2060–2061.

(56) Guerrero, G.; Mutin, P. H.; Vioux, A. *J. Mater. Chem.* **2001**, *11*, 3161–3165.

(57) Cinausero, N.; Azema, N. *Polym. Adv. Technol.* **2008**, 701–709.

(58) Cinausero, N.; Azema, N.; Cuesta, J.-M. L.; Cochez, M.; Ferriol, M. *Polym. Adv. Technol.* **2011**, *22*, 1931–1939.

(59) Keene, T. D.; Price, D. J.; Kepert, C. J. *Dalton Trans.* **2011**, *40*, 7122–7126.

(60) McCusker, L. .; Baerlocher, C.; Jahn, E.; Buelow, M. *Zeolites* **1991**, *11*, 308–313.

***Note that this reference is the supporting information for the paper referenced as (41), which describes in detail experimental procedures

5.2 – Sample databases

5.2.1 – VPI-5 - Synthesis

Sample ID	Molar equiv water added		Stir speed / RPM		Ageing time / min	
	Step 1	Step 2	Step 1	Step 2	Step 1	Step 2
8	35	55	550	1100	90	30
9	35	55	550, 600	1100, 1200	90	30
10	35	55	1200, 1500	1500	100	1440
11	35	55	800, 1500	1500	5	1620
12	35	55	600, 1200	1200	90	30
13	35	55	600, 1200	1200	90	30
14	36.7	58.7	-	600	90	30
15	36.7	58.7	1500	1500	90	30
16	36.7	58.7	600	600	100	30
17	36.7	58.7	600	350	80	30
18	36.7	58.7	600	700	96	30
19	36.7	58.7	-	450	100	40
20	36.7	58.7	650	600	90	30
21	36.7	58.7	600	1200	90 (60 sonic)	30
22	36.7	58.7	600	600	90 (60 sonic)	30
23	36.7	58.7	600	600	90	30
24	36.7	58.7	150	300	90	30
25	36.7	58.7	-	400	90	30
26	36.7	58.7	-	400	90	30
27	36.7	58.7	-	400	90	30
28	36.7	58.7	-	400	90	30

Sample ID	Crystallisation temp / deg	SDA	Sonicated	Manual grinding	Stirrer bar size	Ortho/Poly PPA
8	140	DPA	Y	N	S	Ortho
9	140	DPA	Y	N	S	Ortho
10	130	DPA	N	N	S	Ortho
11	140	DPA	N	N	S	Ortho
12	123	DPA	N	N	L	Ortho
13	123	DPA	N	N	S	Ortho
14	123	DPA	Y	Y	S	Ortho
15	123	DPA	N	N	S	Ortho
16	123	DPA	N	N	L	Ortho
17	123	DPA	Y	N	L	Ortho
18	123	DPA	N	N	L	Ortho
19	123	DPA	Y	Y	L	Ortho
20	140	DPA	Y	N	L	Ortho
21	140	DPA	Y	N	S	Ortho
22	140	DBA	Y	N	L	Ortho
23	140	DPA	Y	N	S	Poly
24	140	DPA	Y	N	L	Poly
25	135	DPA	Y	Y	L	Poly
26	135	DPA	Y	Y	L	Poly
27	123	DPA	Y	Y	L	Poly
28	125	DPA	Y	Y	L	Poly

5.2.2 – VPI-5 – Dehydration

Sample ID	Temperature / deg (stage 1)	Vacuum (stage 1)	Time / h (stage 1)	Molecular sieves?	Temperature / deg (stage 2)	Time / h (stage 2)	Phase retention
25d	80	N	24	Y	-	-	
25c	180	N	24	N	-	-	
29	60	Y	3	N	-	-	
30	23	Y	1	Y	100	1	
32	23	Y	4	N	100	1	
33	23	Y	8	N	-	-	
34	-1	Y	24	N	-	-	
35	-18	Y	5	N	-		
36	-4	Y	5	N	-	-	
37	-4	Y	4	N	23	3	
38	-4	Y	4	N	100	3	

5.2.2 – Sample database – SL-1

Sample ID	Piranha etch/ mins	Crystallisation temp/ deg	Crystallisation time/ h	Vol water / ml
48	0	180	48	14.0
49	10	180	48	14.0
50	30	180	48	14.0
56	0	130	24	14.0
57	10	130	24	14.0
58	30	130	24	14.0
61	0	130	24	7.0
62	0	130	24	3.5